THE JOURNAL OF BIOLOGICAL CHEMISTRY VOL. 289, NO. 33, pp. 22815–22834, August 15, 2014

The Subfamily-specific Assembly of Eag and Erg K^+ Channels Is Determined by Both the Amino and the Carboxyl Recognition Domains*

Received for publication, May 2, 2014, and in revised form, June 24, 2014 Published, JBC Papers in Press, July 9, 2014, DOI 10.1074/jbc.M114.574814

Ting-Feng Lin[‡1], I-Wen Lin[‡1], Shu-Ching Chen[§], Hao-Han Wu[‡], Chi-Sheng Yang[‡], Hsin-Yu Fang[‡], Mei-Miao Chiu[‡], and Chung-Jiuan Jeng[‡¶2]

From the [‡]Institute of Anatomy and Cell Biology, School of Medicine, and the [¶]Brain Research Center, National Yang-Ming University, No. 155, Section 2, Li-Non Street, Taipei 12212, Taiwan and the [§]Department of Medical Research, National Taiwan University Hospital, Taipei 10051, Taiwan

Background: K^+ channel subunits from different ether-à-go-go subfamilies cannot form heterotetramers.
Results: Reversal of subfamily specificity was only possible when we exchanged both amino and carboxyl termini between two ether-à-go-go subunits.
Conclusion: Both recognition domains are required for subfamily-specific assembly.
Significance: This is the first evidence suggesting that the amino terminus of ether-à-go-go K^+ channels governs subunit interaction specificity.

A functional voltage-gated K^+ (Kv) channel comprises four pore-forming α-subunits, and only members of the same Kv channel subfamily may co-assemble to form heterotetramers. The ether-à-go-go family of Kv channels (KCNH) encompasses three distinct subfamilies: Eag (Kv10), Erg (Kv11), and Elk (Kv12). Members of different ether-à-go-go subfamilies, such as Eag and Erg, fail to form heterotetramers. Although a short stretch of amino acid sequences in the distal C-terminal section has been implicated in subfamily-specific subunit assembly, it remains unclear whether this region serves as the sole and/or principal subfamily recognition domain for Eag and Erg. Here we aim to ascertain the structural basis underlying the subfamily specificity of ether-à-go-go channels by generating various chimeric constructs between rat Eag1 and human Erg subunits. Biochemical and electrophysiological characterizations of the subunit interaction properties of a series of different chimeric and truncation constructs over the C terminus suggested that the putative C-terminal recognition domain is dispensable for subfamily-specific assembly. Further chimeric analyses over the N terminus revealed that the N-terminal region may also harbor a subfamily recognition domain. Importantly, exchanging either the N-terminal or the C-terminal domain alone led to a virtual loss of the intersubfamily assembly boundary. By contrast, simultaneously swapping both recognition domains resulted in a reversal of subfamily specificity. Our observations are consistent with the notion that both the N-terminal and the C-terminal recognition domains are required to sustain the subfamily-specific assembly of rat Eag1 and human Erg.

In neurons, a variety of different voltage-gated K^+ (Kv)[3] channels are essential for setting membrane excitability, controlling firing frequencies, and determining the falling phase of action potentials (1, 2). A functional Kv channel comprises four pore-forming α-subunits (3, 4). Based on the sequence analysis of α-subunits, Kv channels are divided into 12 major subfamilies (Kv1–Kv12) (5). In general, only members of the same Kv channel subfamily may co-assemble to form functional heterotetramers (6–10). This subfamily-specific formation of tetrameric K^+ channels requires specific intersubunit associations via recognition or stabilization domains located within individual α-subunits. In Kv1 channels, for example, the cytoplasmic N-terminal tetramerization domain (T1 domain) plays an important role in both subunit tetramerization and subfamily-specific assembly (8, 10, 11).

The ether-à-go-go family of K^+ channels (KCNH) encompasses three distinct Kv subfamilies: Eag (Kv10), Erg (Kv11), and Elk (Kv12) (12). Members of different ether-à-go-go subfamilies, such as Eag and Erg, fail to form heterotetramers (13). A stretch of 41 amino acids in the distal end of the C terminus of Eag α-subunits has been suggested to have a high probability of forming coiled-coil structure and may contribute to subunit assembly; this region is hence termed the carboxyl assembly domain (CAD) (14, 15). A similar tetramerizing coiled-coil (TCC) domain is also found in the distal end of the C terminus of Erg α-subunits (15). Interestingly, a chimeric Erg construct, whose TCC domain was replaced by the CAD of Eag, was able to form heteromultimeric channels with Eag (15), raising the possibility that CAD/TCC may serve as the subfamily recognition domain as well.

Much remains to be learned about the assembly of subunits in ether-à-go-go subfamilies. For instance, because the CAD

* This work was supported by research grants from the National Science Council, Taiwan (Grant NSC101-2320-B-010-038-MY3) and from the Aim for the Top University Plan, Ministry of Education, Taiwan.
[1] Both authors contributed equally to this work.
[2] To whom correspondence should be addressed: Institute of Anatomy and Cell Biology, School of Medicine, National Yang-Ming University, No. 155, Section 2, Li-Non St., Taipei 12212, Taiwan. Tel.: 886-2-28267072; Fax: 886-2-28212884; E-mail: cjjeng@ym.edu.tw.

[3] The abbreviations used are: Kv, voltage-gated K^+; CAD, carboxyl assembly domain; CNBHD, cyclic nucleotide-binding homology domain; HEK, human embryonic kidney; hErg, human Erg; rEag1, rat Eag1; T1 domain, tetramerization domain; TCC, tetramerizing coiled-coil.

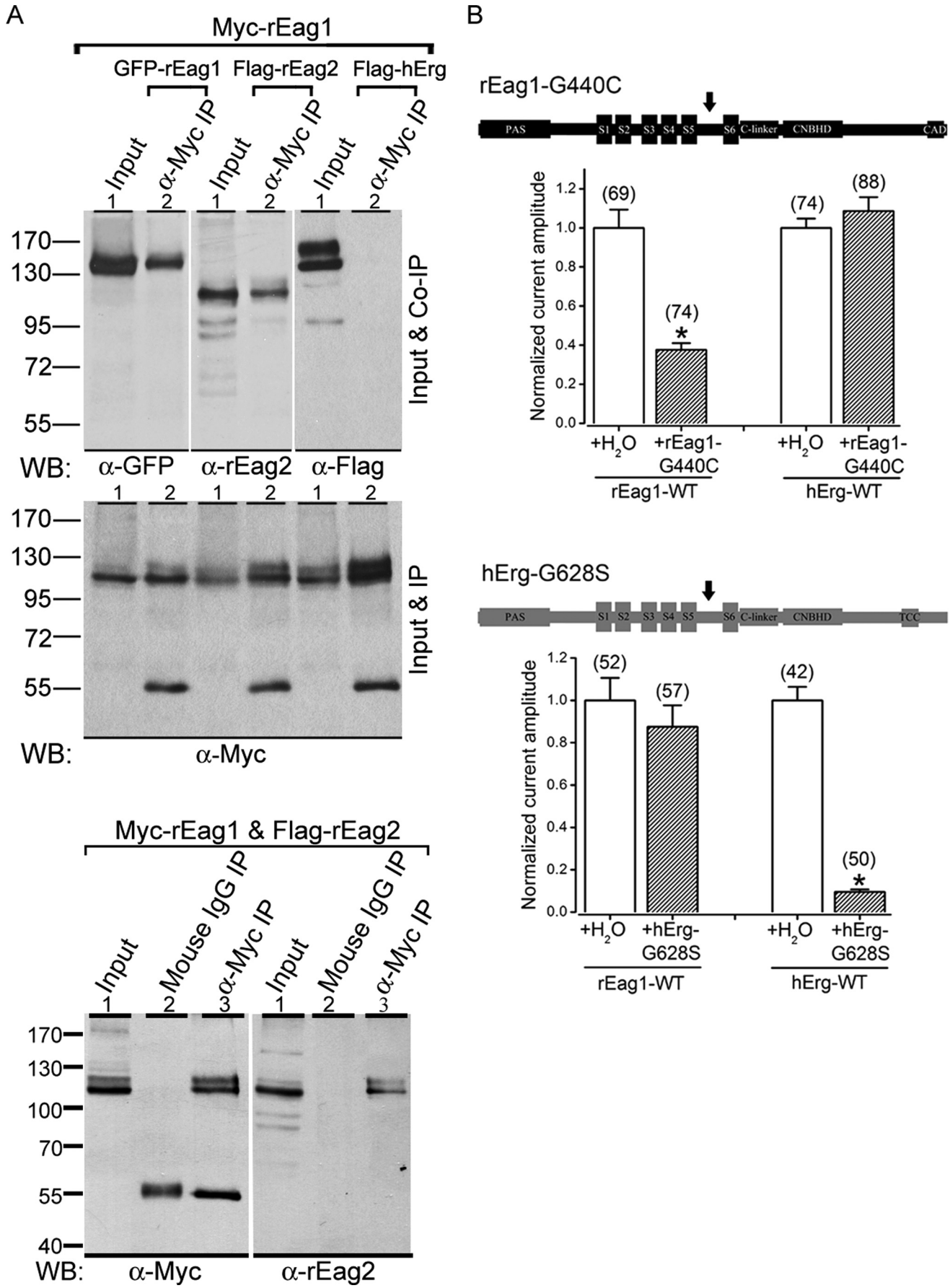
A
Myc-rEag1
GFP-rEag1
Flag-rEag2
Flag-hErg
Input
α-Myc IP
1
2
170
130
95
72
55
Input & Co-IP
WB:
α-GFP
α-rEag2
α-Flag
Input & IP
α-Myc
Myc-rEag1 & Flag-rEag2
Mouse IgG IP
3
100
70
40
α-rEag2
B
rEag1-G440C
PAS
S1
S2
S3
S4
S5
S6
C-linker
CNBHD
CAD
Normalized current amplitude
(69)
(74)
(88)
+H2O
+rEag1-G440C
rEag1-WT
hErg-WT
hErg-G628S
TCC
(52)
(57)
(42)
(50)
+hErg-G628S

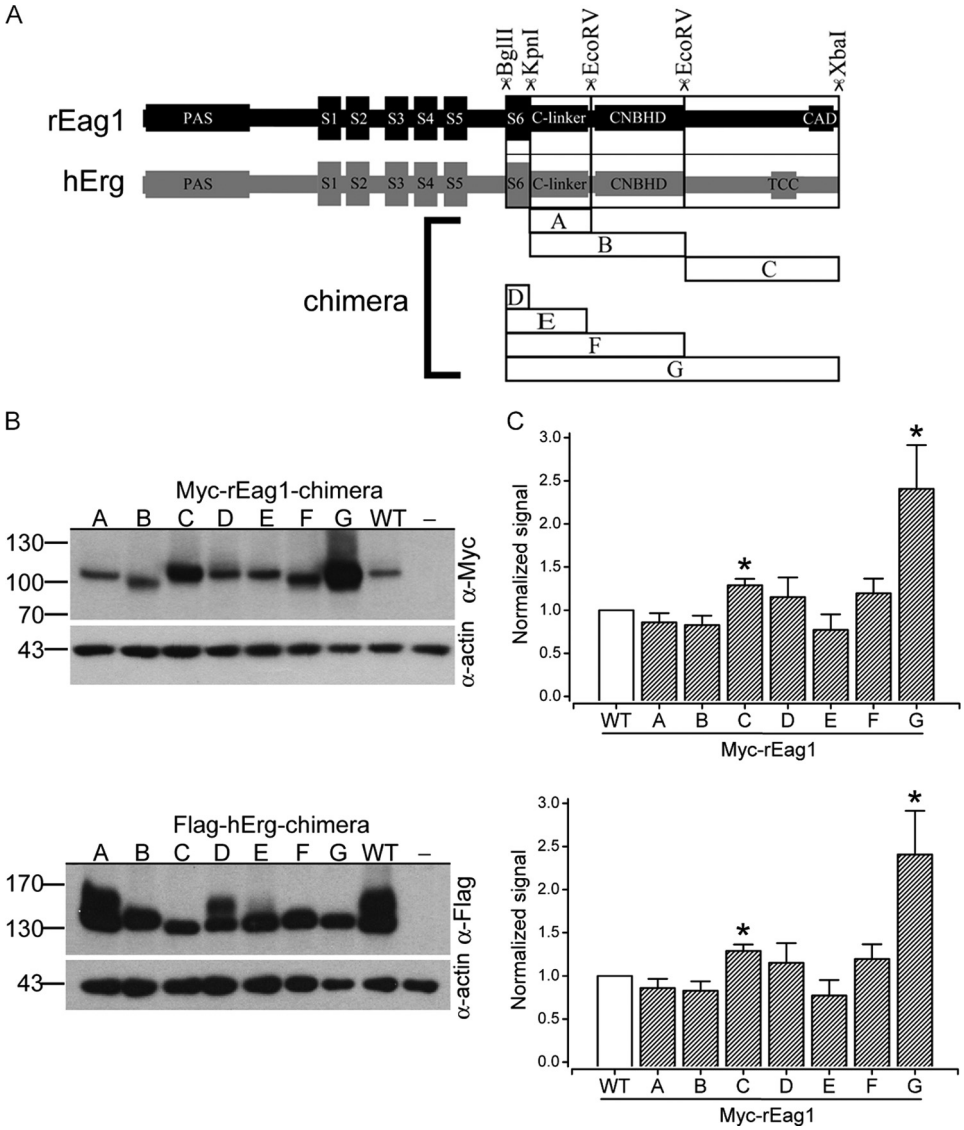

FIGURE 2. **Protein expression of the C-terminal chimeras between rEag1 and hErg channels.** *A*, schematic representation of C-terminal chimeras (for more detail, see "Experimental Procedures"). *B*, representative immunoblots of various Myc-tagged rEag1 (*top*) and FLAG-tagged hErg (*bottom*) chimeras in HEK293T cells. Protein bands were detected with anti-Myc or anti-FLAG antibodies. Also shown are immunoblots of cells transfected with control vectors (−). Corresponding β-actin expression levels for each lane are displayed in the *bottom panels*. *C*, quantification of protein expression levels of Myc-rEag1 (*top*) and FLAG-hErg (*bottom*) chimeras in HEK293T cells. Protein density was standardized as the ratio of Myc or FLAG signal to cognate β-actin signal. Values from various chimeras were then normalized with respect to those of the corresponding WT construct. Densitometric scans of immunoblots were obtained from 3–6 independent experiments. *Asterisks* denote significant difference from the corresponding WT (*, Student's *t* test, $p < 0.05$). *Error bars*, S.E.

and the TCC domain are only about 25 and 85 residues away from the very end of the Eag and the Erg proteins, respectively, it is still unknown how a domain that is translated relatively late can effectively govern subunit assembly and subfamily recognition processes. Most importantly, is CAD/TCC the sole and/or principal assembly and recognition domain for Eag and Erg? Previous truncation analyses from our laboratory indicate that the CAD is not required for the assembly of Eag subunits (16).

FIGURE 1. **Subfamily-specific assembly of rEag1 and hErg subunits.** *A*, biochemical verification of the subfamily-specific interaction of the ether-à-go-go K^+ channel subunits in HEK293T cells. cDNAs for Myc-tagged rEag1 and GFP-rEag1/FLAG-rEag2/FLAG-hErg were co-transfected into HEK293T cells. Cell lysates were immunoprecipitated (*IP*) with the anti-Myc antibody (α-*Myc*). *Top*, GFP-rEag1, FLAG-rEag2, and FLAG-hErg proteins in the lysates (*Input*) or the immunoprecipitates (α-*Myc IP*) were detected by immunoblotting (*WB*) with anti-GFP (α-*GFP*), anti-rEag2 (α-*rEag2*), or anti-FLAG (α-*FLAG*) antibodies. In all cases hereafter, input represents 5% of the total protein used for immunoprecipitation. The positions of mass markers (in units of kDa) are indicated to the *left* of the blots. *Center*, corresponding expression levels of Myc-rEag1 (with an apparent molecular mass of about 110–120 kDa) were examined by immunoblotting with the anti-Myc antibody. *Bottom*, the negative control for immunoprecipitation. Note that co-immunoprecipitation of rEag1 and rEag2 can only be achieved by using the anti-Myc antibody, not the mouse IgG. *B*, subfamily-specific interactions were also exemplified by the dominant negative effects of the non-functional pore mutants rEag1-G440C (*top*) and hErg-G628S (*bottom*) subunits in *Xenopus* oocytes. Oocytes were subject to cRNA injection (in the standard concentration) of WT channel in the presence or absence (replaced with the nuclease-free water, $+H_2O$) of the indicated pore mutant (for more detail, see "Experimental Procedures"). K^+ currents through WT channels were recorded in 3 mM external KCl. For rEag1-WT, steady-state current amplitudes at +60 mV were measured. For hErg-WT, peak tail current amplitudes at −120 mV (in response to +50-mV test pulses) were measured. The *numbers* in the *parentheses* represent the number of oocytes analyzed for each co-expression condition. *Asterisks* denote significant difference from the water co-injection control (*, *t* test, $p < 0.05$). *Error bars*, S.E.

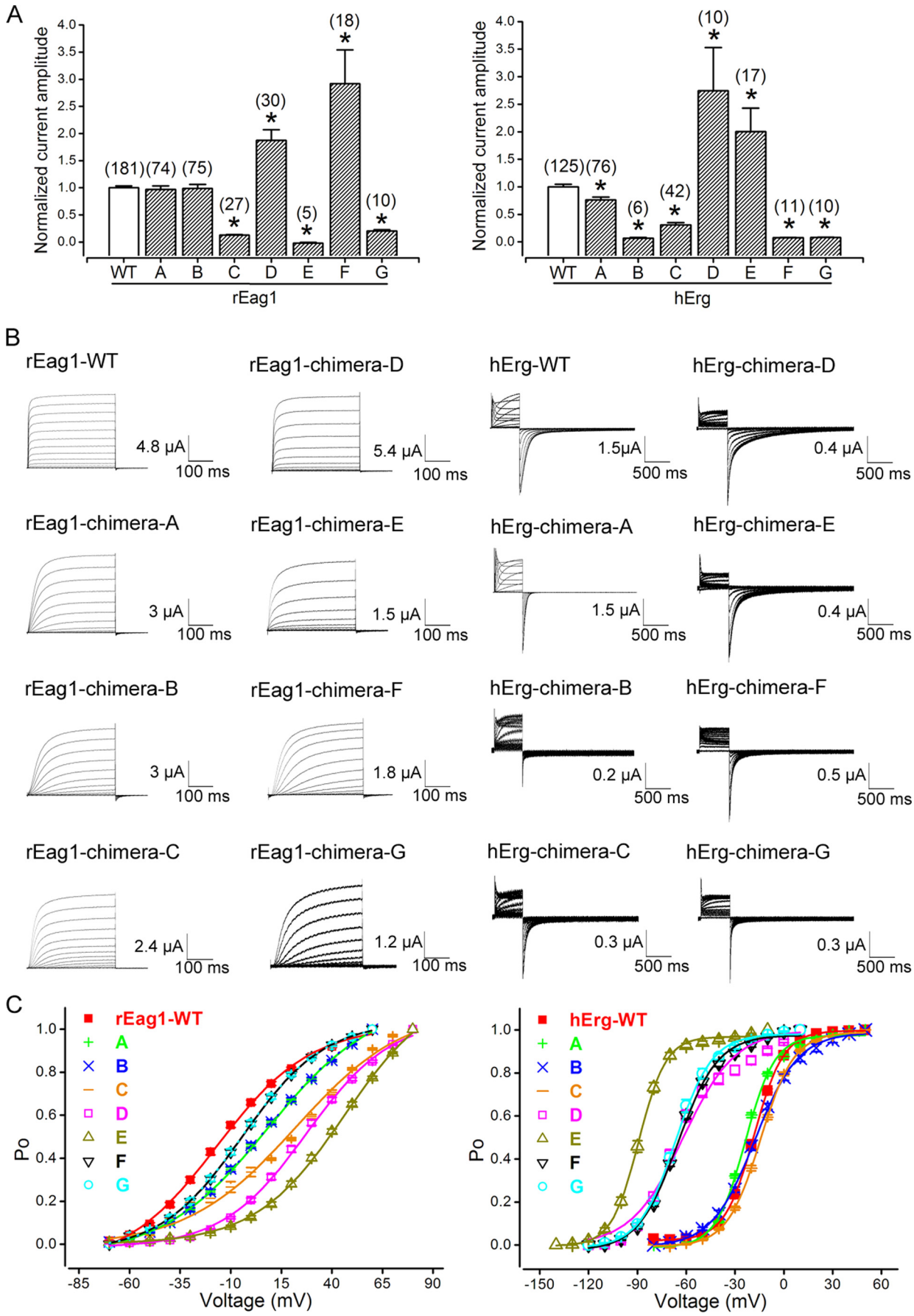
A
Normalized current amplitude
(181)(74) (75) (27) (30) (5) (18) (10)
WT A B C D E F G
rEag1
(125)(76) (6) (42) (10) (17) (11) (10)
hErg
B
rEag1-WT
4.8 μA
100 ms
rEag1-chimera-D
5.4 μA
100 ms
hErg-WT
1.5μA
500 ms
hErg-chimera-D
0.4 μA
500 ms
rEag1-chimera-A
3 μA
100 ms
rEag1-chimera-E
1.5 μA
100 ms
hErg-chimera-A
1.5 μA
500 ms
hErg-chimera-E
0.4 μA
500 ms
rEag1-chimera-B
3 μA
100 ms
rEag1-chimera-F
1.8 μA
100 ms
hErg-chimera-B
0.2 μA
500 ms
hErg-chimera-F
0.5 μA
500 ms
rEag1-chimera-C
2.4 μA
100 ms
rEag1-chimera-G
1.2 μA
100 ms
hErg-chimera-C
0.3 μA
500 ms
hErg-chimera-G
0.3 μA
500 ms
C
Po
rEag1-WT
A
B
C
D
E
F
G
Voltage (mV)
hErg-WT
A
B
C
D
E
F
G
Voltage (mV)

Likewise, subunit interaction for Erg channels may take place in the absence of the TCC domain (17–21). It is therefore possible that other regions within Eag and Erg may also contribute to subunit assembly and subfamily recognition.

In this study, we aim to ascertain the structural basis underlying the subfamily-specific assembly of ether-à-go-go channels. We began by generating a series of different chimeric constructs over the C-terminal region of rat Eag1 (rEag1) and human Erg (hErg) subunits. By performing biochemical and electrophysiological characterizations of the subunit interactions of the chimeras, we demonstrated that the putative assembly domains in the distal C terminus alone were not sufficient to explain their subfamily specificities. Further chimeric analyses over the N-terminal region revealed a hitherto unknown role in governing the specificity of subunit interactions. Our results suggest that both the N- and the C-terminal recognition domains are required for the subfamily-specific assembly of rEag1 and hErg K^+ channels.

EXPERIMENTAL PROCEDURES

cDNA Constructs—rEag1 and rEag2 cDNAs subcloned into pcDNA3 (Invitrogen) were kindly provided by Dr. Olaf Pongs (Zentrum fur Molekulare Neurobiologie, Hamburg, Germany). hErg (hErg 1a) cDNA subcloned into pSP64-poly(A) was kindly provided by Dr. Gail A. Robertson (University of Wisconsin, Madison, WI). To create epitope-tagged constructs for biochemical analyses, rEag1 cDNA was switched into either pcDNA3-Myc or pEGFP (Clontech), rEag2 cDNA was transferred into pcDNA3-FLAG, and hErg cDNA was swapped into either pFLAG-CMV2 (Sigma) or pEGFP. pcDNA3- and pSP64-based constructs were used for heterologous expression in *Xenopus* oocytes; pcDNA3-, pFLAG-CMV2-, and pEGFP-based constructs were chosen for heterologous expression in mammalian cells.

The QuikChange site-directed mutagenesis kit (Stratagene) was used to produce the following mutant constructs. G440C and G628S pore mutants were created for rEag1 and hErg, respectively. A premature stop codon (denoted by X) was introduced at Asn-861 or Arg-1032 to generate the truncated hErg constructs N861X and R1032X. As summarized below, chimeric constructs were generated by introduction of compatible restriction sites in both rEag1 and hErg through silent or missense mutations: chimera A, KpnI (rEag1-N481G/T482T; hErg-G669G/T670T) and EcoRV#1 (rEag1-A558I/S559S; hErg-A746I/T747S); chimera B, KpnI and EcoRV#2 (rEag1-I678I/V679S; hErg-N886I/M887S); chimera C, EcoRV#2 and XbaI (in vectors); chimera D, BglII (removal of one endogenous site at rEag1-I378I, leaving intact the other site at rEag1-Lys-450 and Ile-451; endogenous unique site at hErg-Lys-638 and Ile-639) and KpnI; chimera E, BglII and EcoRV#1; chimera F, BglII and EcoRV#2; chimera G, BglII and XbaI; chimera N, HindIII (in vectors) and PmeI#2 (rEag1-V215V/F216F/K217K/T218L; hErg A408L); chimera O, PmeI#I (rEag1-A135A/K137K; hErg-K135F/D136K/M137L) and PmeI#2; chimera P, HindIII and PmeI#1; N-terminal deletion (ΔN), double digestion with HindIII and PmeI#2, followed by insertion of the triamino acid linker sequence LAG. All constructs were subject to DNA sequencing verification.

Cell Culture and Transfection—Human embryonic kidney (HEK293T) cells were maintained in Dulbecco's modified Eagle's medium (DMEM) supplemented with 2 mM L-glutamine, 100 units/ml penicillin/streptomycin, and 10% (v/v) fetal bovine serum (Hyclone). Cells were maintained at 37 °C in a 95% air and 5% CO_2 humidified incubator and passaged about every 4 days. Transient transfection was performed by standard calcium phosphate methods. Unless stated otherwise, for each construct, about 3 μg of cDNA was added to each well on a 6-well cell culture plate. For co-expression experiments, cDNA co-transfection was conducted in a 1:1 molar ratio (*i.e.* 3 μg + 3 μg of cDNA/well). Two days after transfection, cells were processed for biochemical experiments.

Co-immunoprecipitation and Western Blotting—Transfected HEK293T cells were solubilized in ice-cold immunoprecipitation buffer (20 mM Tris-HCl, pH 7.4, 150 mM NaCl, 10 mM Na_2HPO_4, 1% Triton X-100, 0.5% sodium deoxycholate, 0.1% SDS, 1 mM EDTA, and 1 mM phenylmethylsulfonyl fluoride) containing protease inhibitor mixture (Roche Applied Science). Insolubilized materials were removed by centrifugation. Solubilized lysates were precleared with protein A/G-Sepharose beads (GE Healthcare) for 1 h at 4 °C and then incubated for 16 h at 4 °C with protein A/G-Sepharose beads precoated with appropriate antibodies. Beads were gently spun down and washed three times in immunoprecipitation buffer and twice with TBS (20 mM Tris-HCl, pH 7.4, 150 mM NaCl). The immune complexes were eluted from the beads by boiling for 5 min in SDS sample buffer. Protein in the cell lysates or immunoprecipitated samples was separated on 7.5% SDS-PAGE; transferred to nitrocellulose membranes; and detected using mouse anti-Myc (clone 9E10), rabbit anti-GFP (1:5000; Abcam), mouse anti-FLAG (1:1000; Sigma, clone M2), rabbit anti-FLAG (1:5000; Sigma), mouse anti-β-actin (1:10,000; Sigma), rabbit anti-rEag1 (1:10,000; Alomone), or rabbit anti-rEag2 (1:5000; Alomone) antibodies. Blots were then exposed to horseradish peroxidase-conjugated anti-mouse or anti-rabbit IgG (1:5000; Jack-

FIGURE 3. **Functional expression of rEag1 and hErg C-terminal chimeric channels.** *A*, the relative mean K^+ current amplitudes (3 mM external KCl) measured from oocytes injected with the cRNA (0.1 μg/μl) for various constructs of rEag1 (*left*) and hErg (*right*) channels. For rEag1, steady-state current amplitudes at +60 mV were measured. For hErg, peak tail current amplitudes at −120 mV (in response to +50-mV test pulses) were measured. *Asterisks* denote significant difference from the corresponding WT (*, Student's *t* test, $p < 0.05$). *B*, representative K^+ current traces recorded from oocytes expressing various constructs of rEag1 (*left panels*) and hErg (*right panels*) channels. In order to perform detailed biophysical analyses, the cRNA concentrations for some of the low expressing chimeric constructs were increased up to 3 μg/μl. The bath solution contained 3 mM KCl. Depending on the steady-state voltage dependence properties of different constructs, the holding potential was set at −90, −100, or −120 mV. For rEag1, the pulse protocol comprised 370-ms depolarizing test pulses (with 10-mV increments) up to +60/80 mV. For hErg1, the pulse protocol comprised 600-ms depolarizing test pulses (with 10-mV increments) up to +10/50 mV, followed by a tail potential at −100/120/140 mV. *C*, the steady-state activation curves of various constructs of rEag1 (*left*) and hErg (*right*) channels. The fraction of open channels (P_o) was plotted against the corresponding test potential (*V*). Data points were fit with a Boltzmann equation (*solid curves*). For more detail, see Tables 1 and 2. *Error bars*, S.E.

son Immunoresearch Laboratories) and revealed by an enhanced chemiluminescence detection system (WesternBright ECL, Advansta). To enhance the immunoblotting efficiency against the truncation mutants FLAG-hErg-ΔN and FLAG-hErg-ΔN-R1032X, we used the EasyBlot anti-mouse IgG HRP-conjugated second step reagent (GeneTex).

Results shown are representative of at least three independent experiments. Input represents 5% of the total protein used for immunoprecipitation. β-Actin was used as a loading control. Densitometric scans of immunoblots were obtained from at least three independent experiments. Protein signals were quantified by using the ImageJ software (National Institute of Health).

cRNA Preparation and Injection into Xenopus Oocytes—For *in vitro* transcription, rEag1 and hErg cDNA was linearized with XbaI and EcoRI, respectively. Capped cRNA was transcribed *in vitro* from the linearized cDNA template with the mMessage mMachine T7 kit (Ambion). The concentration of cRNA was determined by gel electrophoresis and verified with spectrophotometry.

Adult female *Xenopus laevis* (African *Xenopus* Facility, Knysna, South Africa) were anesthetized by immersion in Tricaine (1.5 g/liter). All procedures were in accordance with the Guidelines for the Care and Use of Mammals in Neuroscience and Behavioral Research (National Research Council 2003) and approved by the Institutional Animal Care and Use Committee of National Yang-Ming University. Ovarian follicles were removed from *Xenopus* frogs, cut into small pieces, and incubated in ND96 solution (96 mM NaCl, 2 mM KCl, 1.8 mM $MgCl_2$, 1.8 mM $CaCl_2$, and 5 mM HEPES, pH 7.5). To remove the follicular membrane, *Xenopus* oocytes were incubated in Ca^{2+}-free ND96 containing collagenase (2 mg/ml) on an orbital shaker (~200 rpm) for about 60–90 min at room temperature. After several washes with collagenase-free, Ca^{2+}-free ND96, oocytes were transferred to ND96. Stage V-VI oocytes were then selected for cRNA injection. Injected oocytes were stored at 16 °C in ND96 solution supplemented with 50 mg/liter gentamycin.

For all cRNA injection paradigms, the total volume of injection was always 41.4 nl/oocyte. To examine the phenotype of individual chimeric and mutant constructs, cRNA concentration up to about 3 μg/μl was used for oocyte injection (*i.e.* up to 124.2 ng of cRNA was injected into an oocyte). For co-expression experiments, it is imperative to find a submaximal cRNA concentration for WT rEag1 and hErg channels that allows us to add an extra amount of mutant cRNA. Therefore, we empirically fixed WT cRNA concentration at 0.1 μg/μl (*i.e.* 4.14 ng of cRNA/oocyte) (16), known as the standard cRNA concentration for oocyte injection. To implement a strict criterion for assessing dominant negative effects of non-functional mutants in the co-expression experiment, the cRNA concentration of mutant constructs was always equal to or less than that of the functional counterpart. Unless stated otherwise, a 1:1 molar ratio (*i.e.* 8.28 ng of cRNA/oocyte) was used for co-expression with hErg-WT. A 1:1 co-injection ratio was also applied for evaluating the dominant negative effects of rEag1 mutants on rEag1-WT. For co-expressing Eag1-WT and hErg mutants, however, the molar ratio 1:0.5 (*i.e.* 6.21 ng of cRNA/oocyte) was chosen because most hErg constructs displayed relatively higher protein expression levels.

TABLE 1

Steady-state voltage-dependent activation parameters of chimeric rEag1 K^+ channels

Except for chimeras N, P, O, and NC, isochronal tail currents recorded with 60 mM external KCl were normalized to the corresponding maximum amplitude to obtain the fraction of open channels (P_o) at the indicated membrane potential. Data points were fit with a Boltzmann equation, $P_o(V) = 1/(1 + \exp((V_{0.5} - V)/k))$, where $V_{0.5}$ is the half-maximal voltage for activation, and k is the slope factor of the P_o-V curve. For chimeras N, P, O, and NC, amplitudes of steady-state currents recorded with 3 mM external KCl were used to calculate channel conductance (G) based on the equation, $G = I \times (V_m - V_{rev})$, where the reversal potential for K^+ (V_{rev}) was assumed to be −90 mV. Normalized G-V curves were fit with a Boltzmann equation, $G(V) = 1/(1 + \exp((V_{0.5} - V)/k))$. Data are shown as mean ± S.E.

Construct	$V_{0.5}$	k	n
	mV		
rEag1-WT	−16.9 ± 1.4	23.1 ± 1.5	61
rEag1-chimera A	8.2 ± 1.0[a]	26.3 ± 1.2	34
rEag1-chimera B	7.8 ± 1.0[a]	26.1 ± 1.1	39
rEag1-chimera C	15.1 ± 2.5[a]	20.6 ± 2.2	3
rEag1-chimera D	27.6 ± 1.2[a]	21.1 ± 1.1	16
rEag1-chimera E	46.2 ± 1.0[a]	21.9 ± 0.6	15
rEag1-chimera F	−4.3 ± 0.3[a]	20.4 ± 0.3	12
rEag1-chimera G	−4.6 ± 0.3[a]	20.4 ± 0.4	10
rEag1-chimera N	−95.2 ± 1.5[a]	15.6 ± 1.3[a]	14
rEag1-chimera P	−49.1 ± 0.4[a]	11.7 ± 0.3[a]	5
rEag1-chimera O	−69.4 ± 1.1[a]	20.3 ± 1.2	5
rEag1-chimera NC	−73.4 ± 1.7[a]	25.6 ± 2.1	12

[a] Significantly different from rEag1-WT; Student's t test, $p < 0.05$.

TABLE 2

Steady-state voltage-dependent activation parameters of chimeric hErg K^+ channels

Isochronal tail currents recorded with 3 mM external KCl were normalized to the corresponding maximum amplitude to obtain P_o-V curves, which were subject to fitting with the Boltzmann equation: $P_o(V) = 1/(1 + \exp((V_{0.5} - V)/k))$.

Construct	$V_{0.5}$	k	n
	mV		
hErg-WT	−18.4 ± 0.1	9.1 ± 0.1	142
hErg-chimera A	−23.7 ± 0.6	9.1 ± 0.6	31
hErg-chimera B	−17.8 ± 0.5	13.3 ± 0.5[a]	5
hErg-chimera C	−14.4 ± 0.2	10.3 ± 0.2	53
hErg-chimera D	−61.4 ± 1.7[a]	16.0 ± 1.5[a]	11
hErg-chimera E	−89.2 ± 0.4[a]	8.4 ± 0.4	16
hErg-chimera F	−65.1 ± 0.8[a]	12.3 ± 0.7[a]	9
hErg-chimera G	−66.6 ± 0.6[a]	11.3 ± 0.5	11
hErg-chimera N	7.8 ± 0.8[a]	11.4 ± 0.7	19
hErg-chimera P	−13.4 ± 0.4	10.5 ± 0.4	11
hErg-chimera NC	5.2 ± 1.1[a]	11.3 ± 1.0	11
hErg-R1032X	−23.2 ± 0.4	9.6 ± 0.3	26

[a] Significantly different from hErg-WT; Student's t test, $p < 0.05$.

Two-electrode Voltage Clamp Recording in Xenopus Oocytes—2–3 days after cRNA injection, oocytes were functionally assayed in a recording bath containing Ringer solution (in 115 mM NaCl, 3 mM KCl, 1.8 mM $CaCl_2$, 10 mM HEPES, pH 7.2). Where indicated, 60 mM KCl was employed (by replacing NaCl) to record tail currents. Niflumic acid (0.5 mM) was added to the bath to minimize the contribution of endogenous Ca^{2+}-activated Cl^- currents. The bath volume was ~200 μl. An agarose bridge was used to connect the bath solution with a ground chamber (containing 3 M KCl) into which two ground electrodes were inserted. Borosilicate electrodes (0.1–1 megaohms) used in voltage recording and current injection were filled with 3 M KCl. K^+ currents through rEag1 channels were acquired, using the conventional two-electrode voltage clamp technique with an OC-725C oocyte clamp (Warner). For the majority of rEag1 channel constructs, passive membrane properties were compensated using the $-P/4$ leak subtraction method provided by the pCLAMP 8.2 software, whereas no leak subtraction was performed for rEag1-chimeras N and P as well as all hErg channel constructs. Data were filtered at 1 kHz (OC-725C oocyte clamp) and digitized at 100 μs/point (10 kHz) using the Digidata 1332A/pCLAMP 8.2 data acquisition system

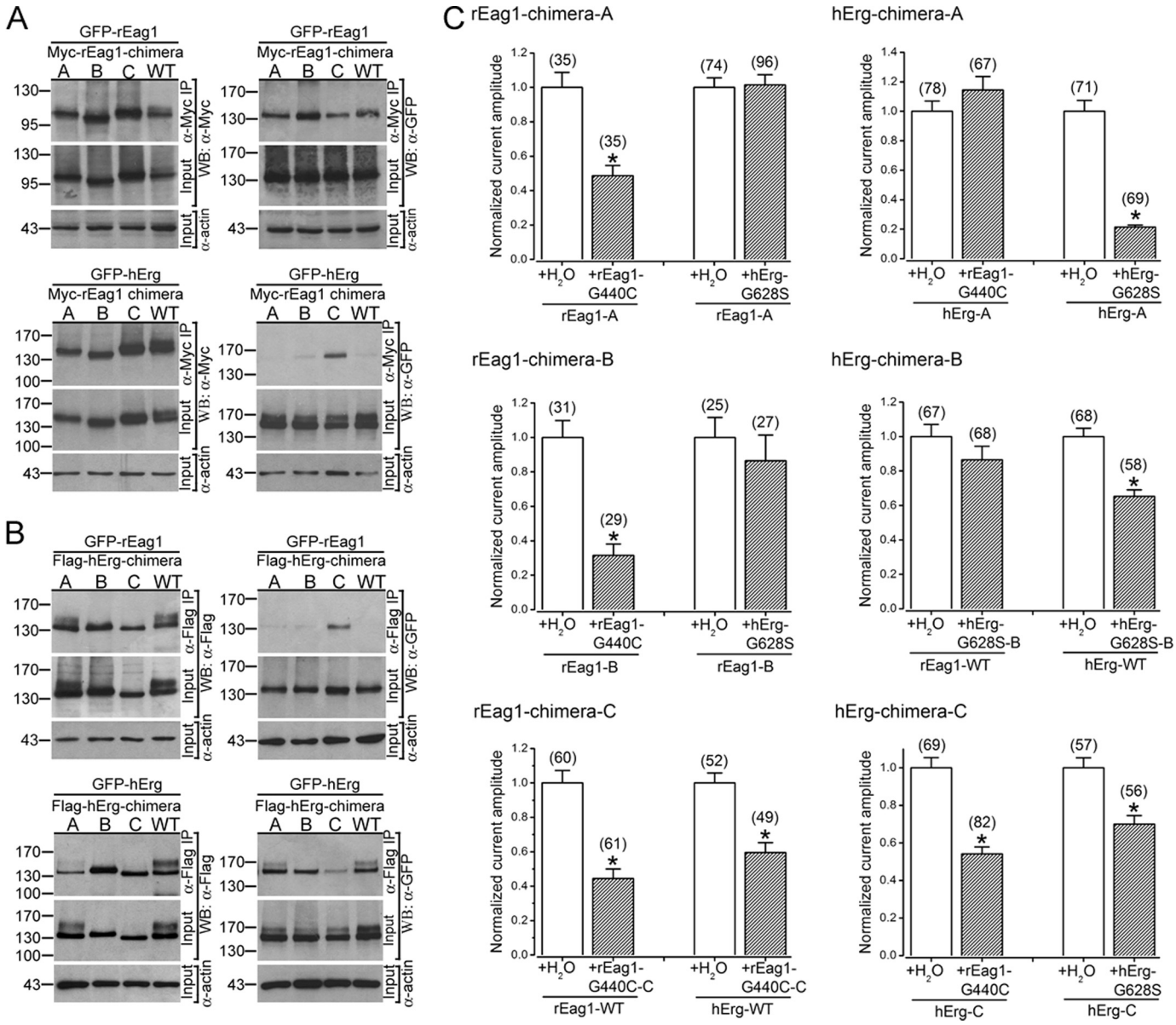

FIGURE 4. **Loss of subfamily specificity for rEag1- and hErg-chimera C.** *A*, biochemical investigation of the subfamily specificity of Myc-rEag1-chimera A, B, and C in HEK293T cells. Each of the indicated Myc-tagged rEag1 constructs was co-expressed with GFP-rEag1-WT (*top panels*) or GFP-hErg-WT (*bottom panels*), and cell lysates were immunoprecipitated (*IP*) with the anti-Myc antibody (*α-Myc*). Myc-rEag1 proteins in the lysates (*Input*) or the immunoprecipitates (*α-Myc IP*) were detected by immunoblotting (*WB*) with the anti-Myc antibody (*left panels*). The corresponding co-immunoprecipitation efficiency of GFP-tagged WT was visualized by immunoblotting with the anti-GFP (*α-GFP*) antibody (*right panels*). *B*, biochemical investigation of the subfamily specificity of FLAG-hErg-chimera A, B, and C in HEK293T cells. Each of the indicated FLAG-tagged hErg constructs was co-expressed with GFP-rEag1-WT (*top panels*) or GFP-hErg-WT (*bottom panels*), and cell lysates were immunoprecipitated with the anti-FLAG antibody (*α-FLAG*). Only chimera Cs were effectively co-immunoprecipitated with both GFP-rEag1-WT and GFP-hErg-WT. *C*, functional examination of the subfamily specificity of rEag1 (*left panels*) and hErg (*right panels*) chimeras in *Xenopus* oocytes. The dominant negative effects of the non-functional pore mutants rEag1-G440C and hErg-G628S were quantified based on the protocols mentioned in Fig. 1*B*. Pore mutations were introduced into the low expressing rEag1-chimera C (*rEag1-G440C-C*) and hErg-chimera B (*hErg-G628S-B*), followed by evaluating their suppression effects on functional WT channels. Only chimera Cs exerted significant dominant negative effects on both rEag1 and hErg channels. *Asterisks* denote significant difference from the water co-injection control (*, Student's *t* test, $p < 0.05$). *Error bars*, S.E.

(Molecular Devices). All recordings were performed at room temperature (20–22 °C). Data analyses were performed via built-in analytical functions of the pCLAMP 8.2 software. For the same batch of oocytes, mean current amplitudes recorded on the same day were normalized with respect to those of the corresponding control condition (*e.g.* WT construct; co-injection with the nuclease-free water). Normalized data from different batches of oocytes or different days of experiments were later pooled together for comprehensive analyses. Results shown are representative of at least 3–5 independent experiments. All values are presented as mean ± S.E. The significance of the difference between two means was tested by Student's *t* test, whereas means from multiple groups were compared by one-way analysis of variance. Statistical analyses were performed with Origin 7.0 software (Microcal Software).

RESULTS

Subfamily-specific Assembly of rEag1 and hErg K^+ Channels—To highlight the subunit interaction property of the ether-à-go-go family, we employed both biochemical and electrophysiological methods to verify the subunit assembly specificity of rEag1 and

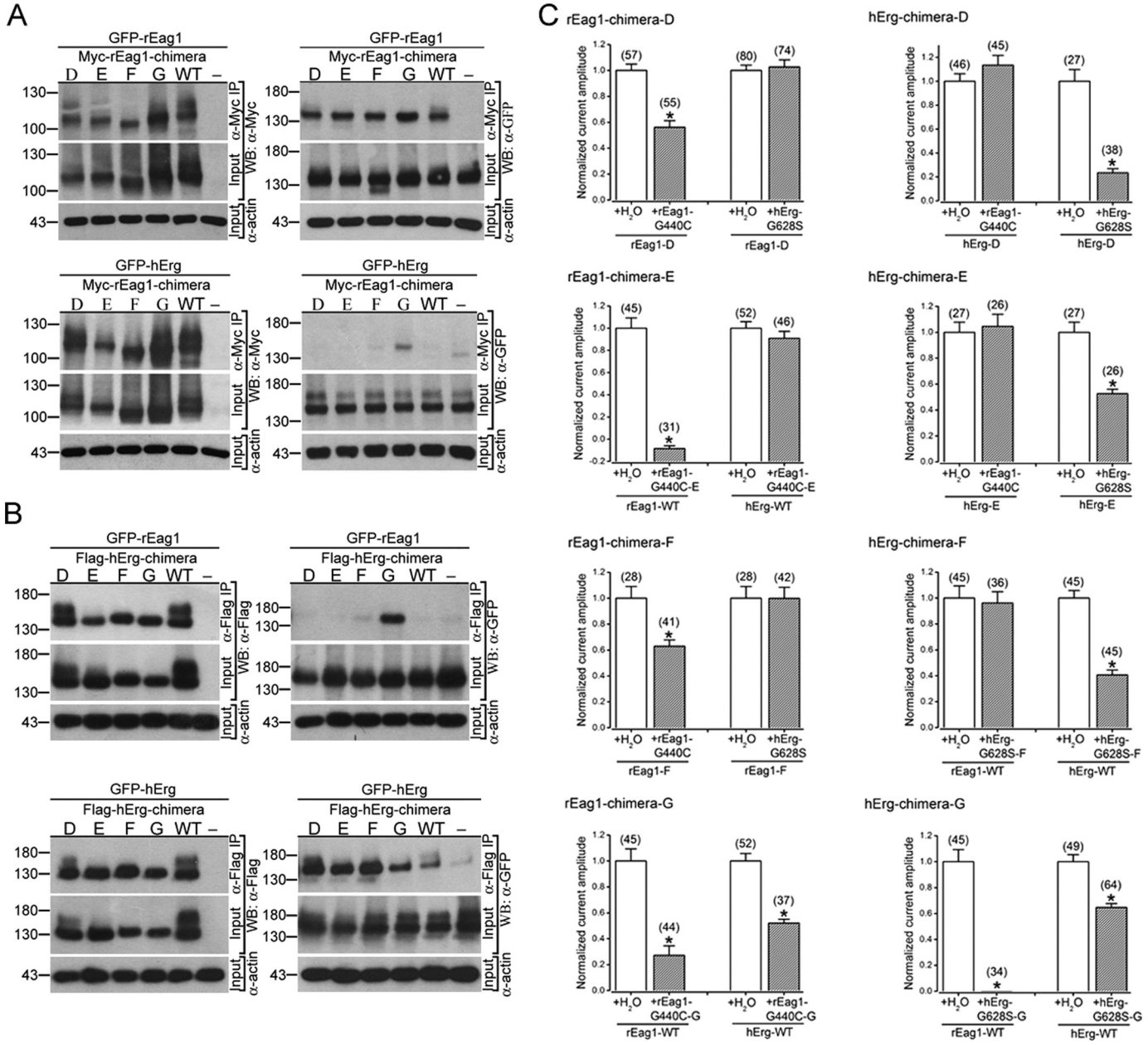

FIGURE 5. **Loss of subfamily specificity for rEag1- and hErg-chimera G.** Biochemical investigations of the subfamily specificity of Myc-rEag1- (*A*) and FLAG-hErg-chimera D, E, F, and G (*B*) were carried out in HEK293T cells. Individual chimeras were co-expressed with GFP-rEag1-WT or GFP-hErg-WT by following the same protocols as outlined in the legend to Fig. 4, *A* and *B*. Also shown are immunoblots of cells transfected with control vectors (−). Only chimera Gs were effectively co-immunoprecipitated with both GFP-rEag1-WT and GFP-hErg-WT. *C*, functional examination of the subfamily specificity of rEag1 and hErg chimeras in *Xenopus* oocytes by quantifying the dominant negative effects of the non-functional pore mutants rEag1-G440C and hErg-G628S. As mentioned in the legend to Fig. 4*C*, pore mutations were introduced into the indicated low expressing rEag1 and hErg chimeras, followed by evaluation of their suppression effects on WT channels. Only chimera Gs exerted significant dominant negative effects on both rEag1 and hErg channels. *Asterisks* denote significant difference from the water co-injection control (*, Student's *t* test, $p < 0.05$). *Error bars*, S.E.

hErg K^+ channels. For biochemical characterization, Myc-tagged rEag1 (Myc-rEag1) was co-expressed with either GFP-tagged rEag1 (GFP-rEag1) or FLAG-tagged hErg (FLAG-hErg) in HEK293T cells for the co-immunoprecipitation experiment. Despite the large size of GFP, previous observations from our laboratory indicated that adding the GFP tag fails to significantly affect the assembly and trafficking of Eag subunits (22). Fig. 1*A* shows that Myc-rEag1 co-existed with GFP-rEag1, but not with FLAG-hErg, in the same protein complex. By contrast, heteromultimer formation was clearly demonstrated upon co-expressing Myc-rEag1 with FLAG-tagged rat Eag2 (FLAG-rEag2), an isoform of the same Eag subfamily.

For electrophysiological characterization, we first generated the non-functional pore mutant G440C and G628S for rEag1 and hErg, respectively (23, 24). We then investigated whether the two non-functional mutants could exert a dominant negative effect on the functional expression of WT rEag1 and hErg K^+ channels. As illustrated in Fig. 1*B*, upon co-expression with rEag1-G440C in *Xenopus* oocytes, the current amplitude of rEag1-WT, but not hErg-WT, was significantly reduced. Conversely, co-expression

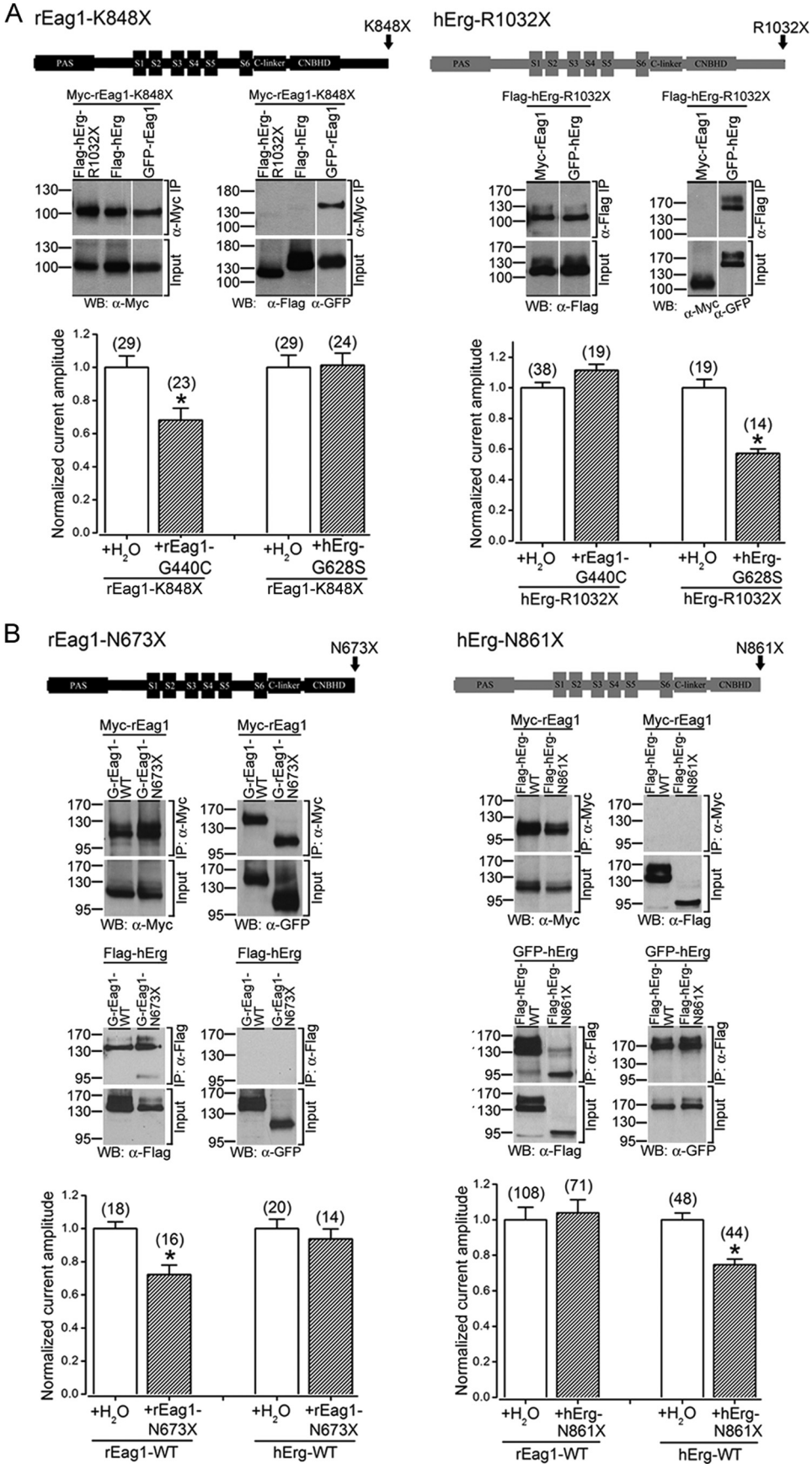
A
rEag1-K848X
K848X
PAS
S1 S2 S3 S4 S5 S6 C-linker CNBHD
Myc-rEag1-K848X
Flag-hErg-R1032X
Flag-hErg
GFP-rEag1
α-Myc IP
Input
WB: α-Myc
WB: α-Flag α-GFP
hErg-R1032X
R1032X
Flag-hErg-R1032X
Myc-rEag1
GFP-hErg
α-Flag IP
WB: α-Flag
WB: α-Myc α-GFP
Normalized current amplitude
(29)
(23)
(29)
(24)
(38)
(19)
(19)
(14)
+H2O
+rEag1-G440C
+hErg-G628S
rEag1-K848X
hErg-R1032X
B
rEag1-N673X
N673X
hErg-N861X
N861X
Myc-rEag1
G-rEag1-WT
G-rEag1-N673X
IP: α-Myc
WB: α-Myc
WB: α-GFP
Flag-hErg
IP: α-Flag
WB: α-Flag
GFP-hErg
Flag-hErg-WT
Flag-hErg-N861X
(18)
(16)
(20)
(14)
(108)
(71)
(48)
(44)
+rEag1-N673X
+hErg-N861X
rEag1-WT
hErg-WT

with hErg-G628S resulted in the suppression of hErg-WT only (Fig. 1*B*). Identical patterns of dominant negative effect were observed when we repeated the same experiments in HEK293T cells (data not shown). Because cRNA injection provided a much more precise control of the molar ratio for co-expression of mutant and WT constructs, thereafter we focused on *Xenopus* oocytes for electrophysiological analyses.

Generation of C-terminal Chimeras—We began by creating a series of seven different chimeric constructs between rEag1 and hErg over the C terminus (Fig. 2*A*): chimera A involved switching the C-linker region; chimera B swapped both the C-linker and the cyclic nucleotide-binding homology domain (CNBHD); chimera C exchanged the post-CNBHD region; chimera D traded the S6 segment; and chimeras E–G gradually extended the range of sequence substitution from "S6-C-linker" to "S6-post-CNBHD" (for more detail, see "Experimental Procedures"). Fig. 2*B* illustrates the representative protein expression patterns of Myc-tagged rEag1 chimeras harboring hErg sequences (Myc-rEag1-chimera A-G), as well as those of FLAG-tagged reverse chimeras (FLAG-hErg-chimera A-G) in HEK293T cells. All chimeric constructs generated a significant amount of channel protein, although some of them showed relatively lower expression levels. Like their WT counterpart, hErg chimeras A and D, and to a lesser extent chimera E, were heavily glycosylated, whereas the other hErg chimeras displayed a significantly reduced glycosylation pattern.

We also examined the functional phenotype of the chimeras. Upon expression in *Xenopus* oocytes (by injecting with the standard 0.1 μg/μl cRNA; for more detail, see "Experimental Procedures"), all chimeric constructs yielded functional K^+ channels, albeit with a pronounced disparity in the relative current amplitude (Fig. 3*A*). For those chimeras with poor functional expression (rEag1-chimera C, E, G; hErg-chimera B, F, G), considerable K^+ currents were recorded upon increasing the cRNA concentration up to 3 μg/μl (Fig. 3*B*). All chimeras were capable of forming functional channels in HEK293T cells as well (data not shown). The general current shapes of the chimeras were similar to those of their WT counterparts: all rEag1 chimeras displayed typical outward K^+ currents with no apparent inactivation, whereas all hErg chimeras exhibited the characteristic inactivation in response to strong membrane depolarizations (Fig. 3*B*). Moreover, hyperpolarization-induced delay in channel activation, a trademark gating property of the Eag K^+ channel subfamily, was also observed in all rEag1 chimeras (data not shown).

The impact of chimeric substitution on channel gating properties, however, differs between rEag1 and hErg. Compared with rEag1-WT, the steady-state activation curves of rEag1-chimera A-G were predominantly right-shifted (Fig. 3*C* and Table 1), with rEag1-chimera E showing a striking shift of about 60 mV. On the contrary, hErg chimera D-G showed left-shifted activation curves (Fig. 3*C* and Table 2), with hErg-chimera E demonstrating a conspicuous change of more than 70 mV. Accordingly, the apparent gating kinetics of some of the chimeras was notably affected. For example, introduction of hErg C-terminal sequences decelerated both the activation and the deactivation kinetics of rEag1, with rEag1-chimeras F displaying the most dramatic change (data not shown). In contrast, hErg chimera A and B exhibited accelerated deactivation kinetics, whereas hErg-chimera D and E showed remarkably slower deactivation kinetics (data not shown).

C-terminal Assembly Domains Are Inadequate to Determine Subfamily-specific Assembly—At least three structural domains in the C-terminal region may be involved in mediating subunit interactions: the C-linker (25), the CNBHD (26), and the post-CNBHD region that contains the CAD or the TCC domain (14, 15). In particular, CAD/TCC was previously suggested to serve as the subunit assembly domain as well as the subfamily recognition domain (14, 15). We therefore asked whether the C-terminal region constitutes the sole or principal recognition domain for subfamily specificity of Eag and Erg channels. To address this issue, we studied the subunit interaction property of various chimeras. As mentioned above (see Fig. 1), upon co-expressing a chimeric channel with its WT counterpart in a 1:1 molar ratio, the presence of potential subunit assembly was verified with the co-immunoprecipitation experiment in HEK293T cells and with the dominant negative assay (in the standard cRNA concentration) in *Xenopus* oocytes. In order to acquire reliable non-functional subunits suitable for dominant negative assays, pore mutations (G440C for rEag1; G628S for hErg) were introduced into those chimeras with poor functional expression (*e.g.* rEag1-chimera C, E, G; hErg-chimera B, F, G) (see Fig. 3), which were subject to co-expression with WT constructs in oocytes. On the other hand, for the other C-terminal chimeras showing vigorous K^+ channel activities, pore mutants in the WT background were employed for cRNA co-injections.

We first investigated the subunit interaction property of chimeras A (C-linker), B (C-linker and CNBHD), and C (post-CNBHD). As illustrated in Fig. 4, both biochemical and electrophysiological analyses indicated that neither chimera As nor chimera Bs notably changed the subfamily-specific assembly of rEag1 and hErg channels. By contrast, in agreement with the

FIGURE 6. **Subfamily-specific assembly of CAD/TCC-lacking C-terminal truncation mutants.** *A*, *top panels*, schematic representation of the C-terminal truncation constructs rEag1-K848X and hErg-R1032X. Both mutants lack the distal post-CNBHD region. *Center panels*, biochemical investigation of the subfamily specificity of the truncation mutants in HEK293T cells. Myc-rEag1-K848X was co-expressed with FLAG-hErg-R1032X, FLAG-hErg-WT, or GFP-rEag1-WT, and cell lysates were immunoprecipitated with the anti-Myc antibody (*left*). Myc-rEag1-K848X could not be effectively co-immunoprecipitated with either FLAG-hErg-R1032X or FLAG-hErg-WT. A parallel experiment was performed by co-expressing FLAG-hErg-R1032X with Myc-rEag1-WT or GFP-hErg-WT, followed by immunoprecipitation with the anti-FLAG antibody (*right*). *Bottom panels*, functional examination of the subfamily specificity of the truncation mutants in *Xenopus* oocytes by quantifying the dominant negative effects of the non-functional pore mutants rEag1-G440C and hErg-G628S. *B*, *top panels*, schematic representation of the C-terminal truncation constructs rEag1-N673X and hErg-N861X. Both mutants lack the complete post-CNBHD region. *Center panels*, GFP-rEag1-N673X was co-expressed with Myc-rEag1-WT or FLAG-hErg-WT for co-immunoprecipitation experiments in HEK293T cells (*left*). The parallel experiment was implemented by co-expressing FLAG-hErg-N861X with Myc-rEag1-WT or GFP-hErg-WT (*right*). The C-terminal truncation mutants could be effectively co-immunoprecipitated with WT subunit of the same subfamily only. *Bottom panels*, because both rEag1-N673X and hErg-N861X failed to produce functional K^+ channels (up to 3 μg/μl cRNA injection) in *Xenopus* oocytes, they were directly co-expressed with either rEag1-WT or hErg-WT for dominant negative assays. All four C-terminal truncation mutants retained their native subfamily-specific suppression properties. *Asterisks* denote significant difference from the water co-injection control (*, Student's *t* test, $p < 0.05$). *Error bars*, S.E.

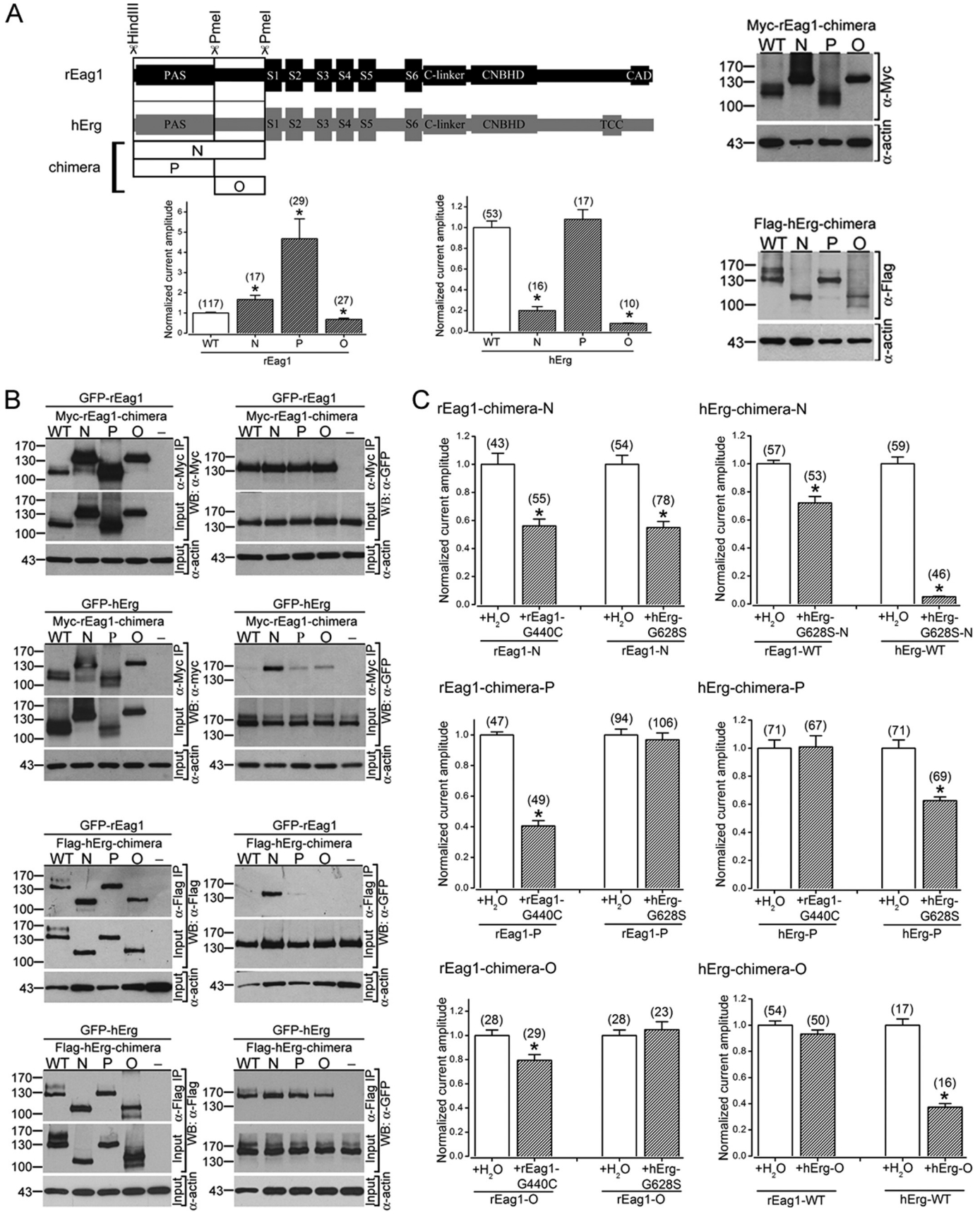
A
HindIII
PmeI
PmeI
rEag1
hERG
chimera
PAS
S1 S2 S3 S4 S5
S6
C-linker
CNBHD
CAD
TCC
N
P
O
Myc-rEag1-chimera
WT N P O
α-Myc
α-actin
Flag-hErg-chimera
α-Flag
Normalized current amplitude
rEag1
hErg
B
GFP-rEag1
Myc-rEag1-chimera
GFP-hErg
Flag-hErg-chimera
IP: α-Myc
WB: α-Myc
WB: α-GFP
IP: α-Flag
WB: α-Flag
Input
α-actin
C
rEag1-chimera-N
hErg-chimera-N
rEag1-chimera-P
hErg-chimera-P
rEag1-chimera-O
hErg-chimera-O
+H2O
+rEag1-G440C
+hErg-G628S
+hErg-G628S-N
+hErg-O
rEag1-N
rEag1-WT
hErg-WT
rEag1-P
hErg-P
rEag1-O
hErg-WT

previous report by Jenke *et al.* (15) rEag1-chimera C, the chimeric rEag1 channel harboring the hErg post-CNBHD region co-existed in a protein complex with and exerted significant dominant negative effect on hErg-WT (Fig. 4, *A* and *C*). Similarly, hErg-chimeric C displayed a prominent interaction with rEag1-WT as well (Fig. 4, *B* and *C*). These results seemed to suggest that the two chimera Cs reversed their respective subfamily specificity. Nevertheless, as exemplified by their reduced but notable co-immunoprecipitation efficiencies and dominant negative effects, rEag1-chimera C and hErg-chimera C were still capable of interacting with rEag1-WT and hErg-WT, respectively (Fig. 4). These findings imply that rather than reversing specificity, the two chimera Cs may instead lose their subfamily specificity.

Given its role in the tetrameric organization of the pore region, the transmembrane S6 segment may also contribute to subunit assembly in rEag1 and hErg channels. Because none of chimeras A through C involved switching the S6 segment, an alternative explanation to the foregoing results is that the subfamily recognition capacity of the post-CNBHD region may somehow be ineffective or even defective in the absence of a homologous S6 segment. To test this hypothesis, we investigated the subunit interaction property of the chimeras that exchanged the S6 segment: chimera D (S6 only), E (from S6 through C-linker), F (from S6 through CNBHD), and G (from S6 through post-CNBHD). Both biochemical and electrophysiological analyses in Fig. 5 demonstrated that for rEag1-chimera D–G, only the post-CNBHD-switching chimera G showed a noteworthy interaction with hErg-WT. Likewise, for hErg-chimera D–G, only chimera G effectively co-existed in a protein complex with rEag1-WT (Fig. 5). Most importantly, exactly like chimera Cs, both chimera Gs still retained significant subunit interaction with their respective "native" subfamily (Fig. 5). Together these data strongly argue that exchanging the post-CNBHD region between the two ether-à-go-go K^+ channel subfamilies does not result in a reversal of subfamily specificity but rather leads to a virtual loss of the intersubfamily boundary.

If the aforementioned inference is true, then it may imply that the post-CNBHD region is not the only or principal subfamily recognition domain for rEag1 and hErg channels. To address this possibility, we inspected the subfamily specificity of four truncation mutants lacking CAD/TCC; rEag1-K848X and hErg-R1032X retained the proximal portion of the post-CNBHD region (Fig. 6*A*), whereas rEag1-N673X and hErg-N861X contained virtually none of the post-CNBHD region (Fig. 6*B*). The truncation mutants rEag1-K848X and hErg-R1032X produced functional K^+ channels with biophysical properties similar to those of respective WT (16) (data not shown). By contrast, neither rEag1-N673X nor hErg-N861X generated significant K^+ currents (16, 17). Despite the absence of CAD/TCC, all of the four truncation mutants preserved their native subfamily-specific assembly properties (Fig. 6), suggesting that indeed CAD/TCC may be dispensable for the subunit-specific assembly of rEag1 and hErg channels.

N-terminal Regions Also Contribute to Subfamily-specific Assembly—If we define the role of a recognition or stabilization domain as being able to effectively promote the assembly of structurally compatible ion channel subunits, as has previously been proposed for the T1 domain in Kv1 channels (27), then a reasonable interpretation of the above results would be that both rEag1 and hErg channels may contain additional subfamily recognition domains outside the C-terminal region. The N-terminal region of both the Eag and the Erg subfamilies comprises three structural divisions: the cap sequence, the PAS domain, and the N-linker region that connects the PAS domain with the transmembrane S1 segment (28–31). Despite sharing homologous cap sequence and PAS domain (collectively known as the eag domain), Eag and Erg significantly differ in the length of the N-linker, with the latter being about 190 amino acids longer. Importantly, hErg 1a (the hErg clone employed herein) and the truncated hErg 1b, two isoforms with a size difference of more than 300 amino acids in the N terminus (32, 33), have been shown to form hetero-oligomers mediated by N-terminal interactions (34), raising the possibility that hErg channels may contain certain N-terminal assembly domains. Furthermore, the hErg PAS (eag) domain was suggested to regulate deactivation kinetics via intersubunit interactions (26). We therefore hypothesized that rEag1 and hErg may contain additional subfamily recognition domains in the N terminus. To test this idea, we generated three different types of N-terminal chimeras: chimera N exchanged the complete N terminus; chimera P switched the homologous eag domain; and chimera O swapped the divergent N-linker (Fig. 7*A*) (for more detail, see "Experimental Procedures").

All of the N-terminal chimeras displayed notable protein expression (Fig. 7*A*). Furthermore, except for hErg-chimera O, the N-terminal chimeras produced functional K^+ channels (Fig. 7*A* and Tables 1 and 2). Most importantly, both biochemical and electrophysiological analyses indicated that chimera Ns were effectively co-immunoprecipitated with both rEag1-WT and hErg-WT (Fig. 7, *B* and *C*), suggesting that, comparable with the consequence of switching CAD/TCC, exchanging the complete N terminus seemed to result in the collapse of the intersubfamily boundary. However,

FIGURE 7. **Loss of subfamily specificity for rEag1- and hErg-chimera N.** *A*, schematic representation of N-terminal chimeras (*top right*) (see "Experimental Procedures" for more detail). Also shown are the representative immunoblots and the normalized protein expression levels of various Myc-tagged rEag1 (*top left*) and FLAG-tagged hErg (*bottom left*) chimeras in HEK293T cells as well as their relative mean K^+ current amplitudes (3 mM external KCl) measured from oocytes (0.1 μg/μl cRNA)(*bottom right*). No significant K^+ current was observed for hErg-chimera O when we increased the cRNA concentration up to 3 μg/μl. *Asterisks* denote significant difference from the corresponding WT (*, Student's *t* test, $p < 0.05$). *B*, biochemical investigation of the subfamily specificity of Myc-rEag1 and FLAG-hErg N-terminal chimeras with GFP-tagged WT subunits in HEK293T cells. Immunoprecipitation experiments were performed with anti-Myc or anti-FLAG antibodies. Also shown are immunoblots of cells transfected with control vectors (−). Only chimera Ns were effectively co-immunoprecipitated with both GFP-rEag1-WT and GFP-hErg-WT. Corresponding β-actin expression levels for each *lane* are displayed in the *bottom panels*. *C*, functional examination of the subfamily specificity of rEag1 and hErg chimeras in *Xenopus* oocytes. Except for the non-functional hErg-chimera O, N-terminal chimeras were subject to dominant negative assays in the absence or presence of the non-functional pore mutants rEag1-G440C and hErg-G628S. hErg-chimera O was evaluated for its suppression effects on WT channels. Only chimera Ns exerted significant dominant negative effects on both rEag1 and hErg channels. *Asterisks* denote significant difference from the water co-injection control (*, Student's *t* test, $p < 0.05$). *Error bars*, S.E.

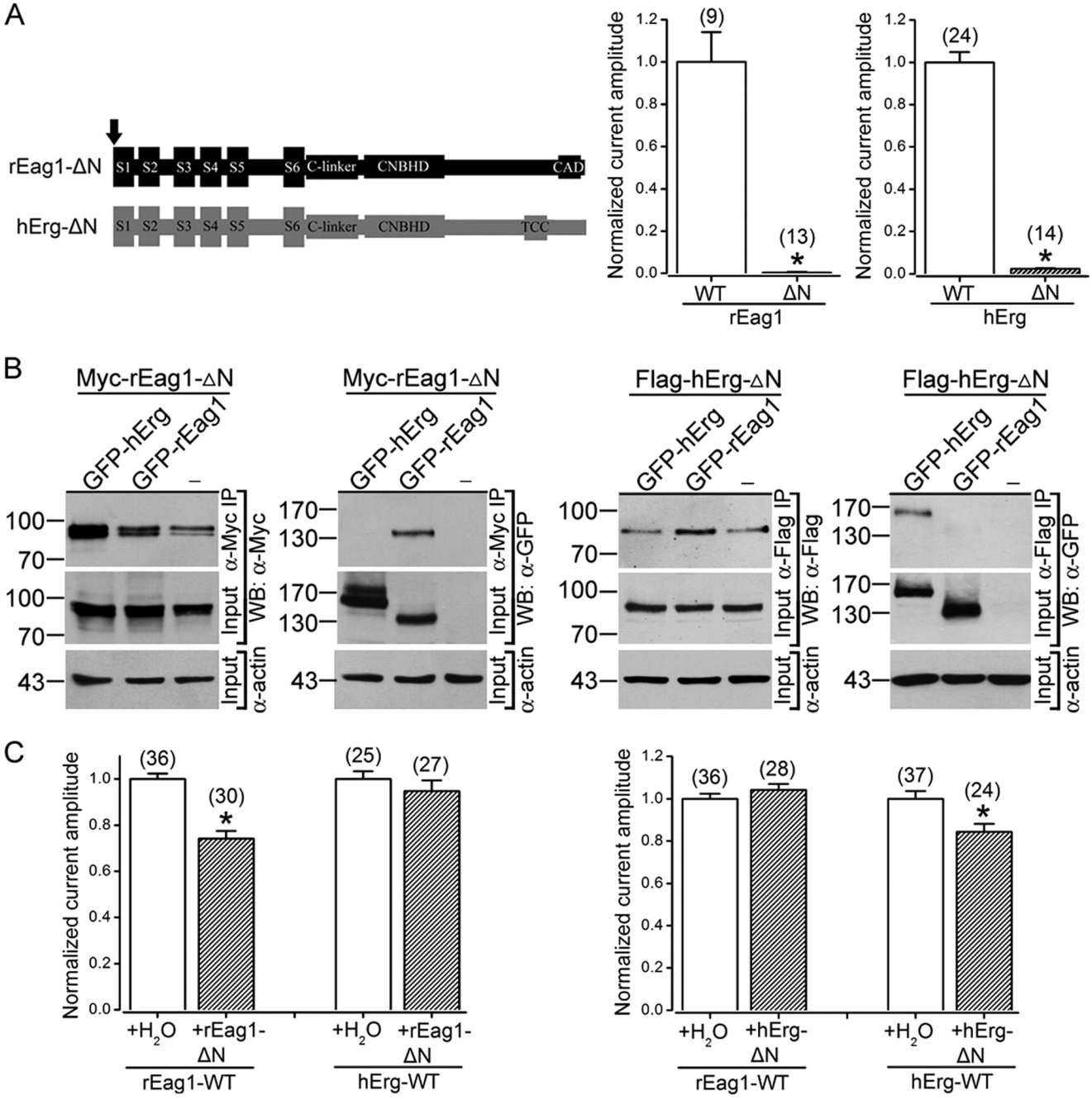

FIGURE 8. **Subfamily-specific assembly of N-terminal truncation mutants.** *A*, *left*, schematic representation of N-terminal truncation (Δ*N*) constructs (for more detail, see "Experimental Procedures"). *Right*, relative mean K^+ current amplitudes (3 mM external KCl) measured from oocytes (0.1 μg/μl cRNA). No significant K^+ current was observed for rEag1-ΔN and hErg-ΔN when we increased the cRNA concentration up to 3 μg/μl. *Asterisks* denote significant difference from the corresponding WT (*, Student's *t* test, $p < 0.05$). *B*, biochemical investigation of the subfamily specificity of Myc-rEag1-ΔN and FLAG-hErg-ΔN with GFP-tagged WT subunits in HEK293T cells. Immunoprecipitation experiments were performed with anti-Myc or anti-FLAG antibodies. Note that N-terminal truncation mutants were effectively co-immunoprecipitated with WT subunit of the same subfamily only. *C*, functional examination of the subfamily specificity of rEag1-ΔN and hErg-ΔN chimeras in *Xenopus* oocytes. The N-terminal mutants were evaluated for their dominant negative effects on WT channels. Both truncation mutants retained their native subfamily-specific suppression properties. *Asterisks* denote significant difference from the water co-injection control (*, Student's *t* test, $p < 0.05$). *Error bars*, S.E.

chimera Ps and chimera Os, both of which involve swapping partial N-terminal sequences, displayed effective interaction with the WT subunit of the same subfamily only (Fig. 7, *B* and *C*). Collectively, the preceding results imply that the N terminus may also contain subfamily recognition domains that presumably comprise a subset of protein sequences entailing both the distal eag domain and the proximal N-linker region.

Exchanging Both the N-terminal and the C-terminal Regions Reverses Subfamily Assembly Specificity—We have already shown that the removal of CAD/TCC failed to affect the subfamily-specific assembly of rEag1 and hErg channels (see Fig. 6). To examine whether the N terminus is indispensable for the subfamily specificity, we also created N-terminal deletion mutants that obliterated the complete N terminus (ΔN) (Fig. 8*A*). As depicted in Fig. 8, for both rEag1 and hErg, removal of

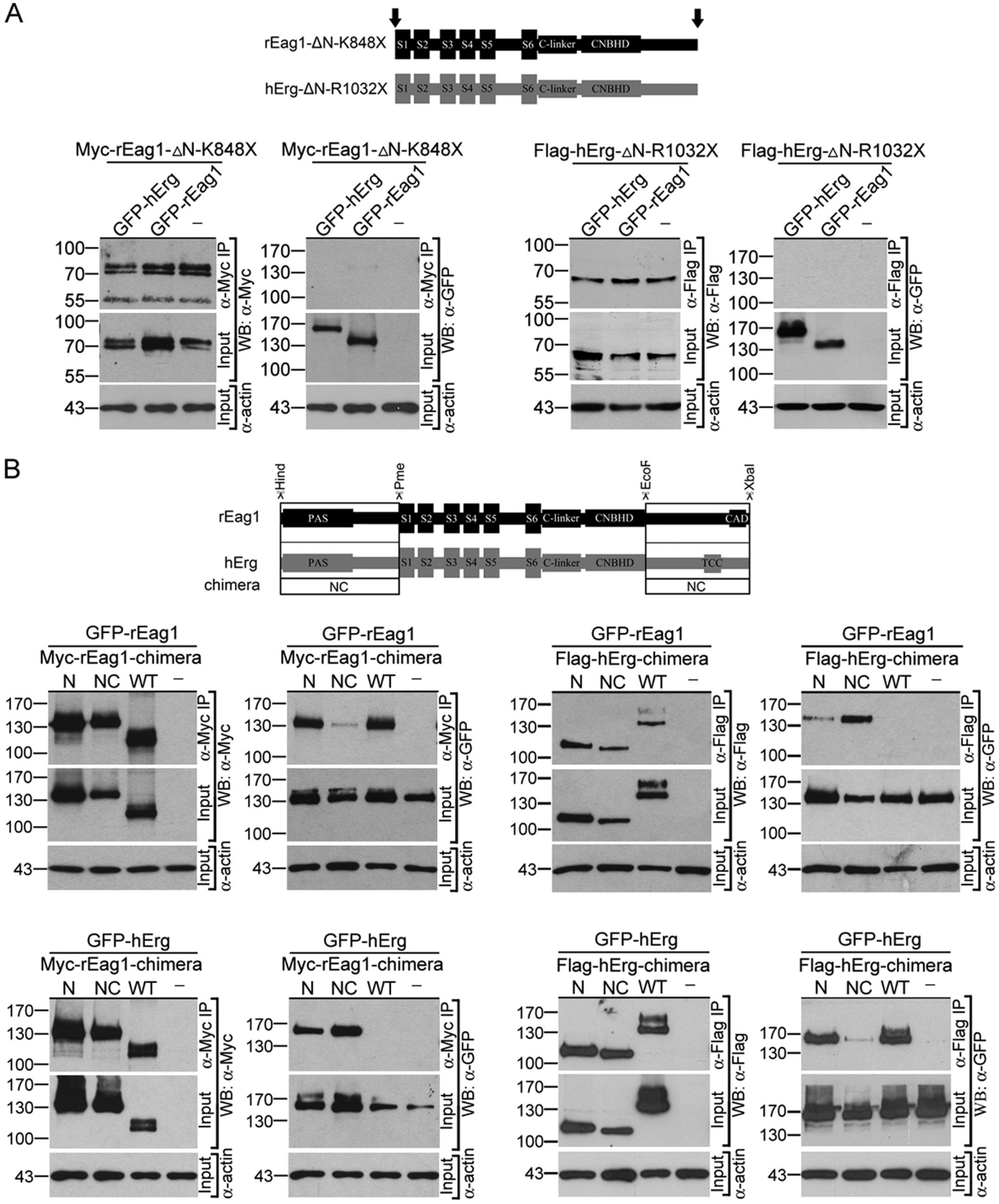

FIGURE 9. **Biochemical characterization of double deletion and double exchange constructs.** *A*, *top*, schematic representation of the double deletion mutants rEag1-ΔN-K848X and hErg-ΔN-R1032X (for more detail, see "Experimental Procedures"). *Bottom*, immunoprecipitation experiments of Myc-rEag1-ΔN/FLAG-hErg-ΔN with GFP-tagged WT subunits in HEK293T cells with anti-Myc or anti-FLAG antibodies. Neither mutants were effectively co-immunoprecipitated with WT subunits. *B*, *top*, schematic representation of the double exchange NC chimeras (for more detail, see "Experimental Procedures"). *Bottom*, immunoprecipitation experiments of Myc-rEag1-ΔN and FLAG-hErg-ΔN. Chimera NCs were more effectively co-immunoprecipitated with the WT subunit from the opposite subfamily.

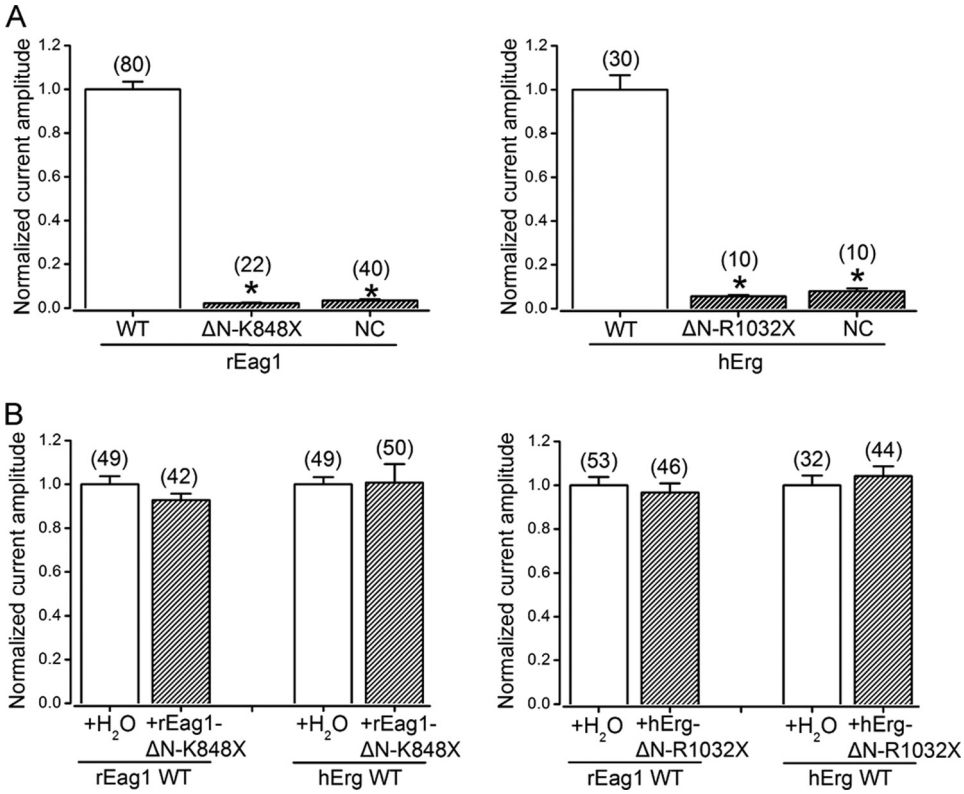

FIGURE 10. **Lack of dominant negative effects for double deletion mutants.** *A*, the relative mean K^+ current amplitudes (3 mM external KCl) of the double deletion the double exchange constructs measured from oocytes (0.1 μg/μl cRNA). When we increased the cRNA concentration up to 3 μg/μl, no significant K^+ current was observed for rEag1-ΔN-K848X and hErg-ΔN-R1032X, whereas small but visible currents were recorded from rEag1- and hErg-chimera NC. *Asterisks* denote significant difference from the corresponding WT (*, Student's *t* test, $p < 0.05$). *B*, dominant negative assays of the double deletion mutants in *Xenopus* oocytes. Neither deletion mutant displayed significant suppression effects on rEag1 or hErg WT channels (Student's *t* test, $p > 0.05$). *Error bars*, S.E.

the entire N-terminal region failed to abolish the subfamily-specific assembly property.

One interpretation of these results is that neither the N-terminal nor the C-terminal region serves as the principal subfamily recognition domain for rEag1 and hErg channels such that we should be looking for other targets over the S1–S6 transmembrane region. Alternatively, one may argue that both the N-terminal and the C-terminal regions may serve as principal and equally important subfamily recognition domains that can take over the subunit discrimination task in the absence of one or the other.

To address these important questions, we first generated double deletion mutants (rEag1-ΔN-K848X and hErg-ΔN-R1032X), in which the entire N terminus as well as CAD/TCC were removed (Fig. 9*A*). The results from co-immunoprecipitation experiments demonstrated that rEag1-ΔN-K848X and hErg-ΔN-R1032X did not appreciably interact with either rEag1-WT or hErg-WT (Fig. 9*A*). Moreover, functional assays indicated that both double deletion mutants were non-functional proteins that failed to exert discernible dominant negative effects on either WT channel (Fig. 10). These observations therefore do not support the idea that the S1–S6 transmembrane region may harbor a potential subfamily recognition domain for rEag1 and hErg channels.

Next, we generated double exchange chimeras (chimera NC), in which both the N terminus and the post-CNBHD region were swapped (Fig. 9*B*). Co-immunoprecipitation studies demonstrated that rEag1-chimera NC co-existed in the same protein complex with hErg-WT (Fig. 9*B*). By contrast, compared with rEag1-chimera N, rEag1-chimera NC was much less effective in interacting with rEag1-WT (Fig. 9*B*). Likewise, in terms of subunit association, hErg-chimera NC displayed a much more prominent preference for rEag1-WT over hErg-WT (Fig. 9*B*). In other words, the two double exchange chimeras seemed to exhibit "reversed" subfamily specificity. To further verify this notion, we went on to look for electrophysiological evidence. Despite the fact that the functional expression of rEag1-chimera NC and hErg-chimera NC was very small in the standard cRNA concentration (Fig. 10*A*), significant K^+ currents were observed when we increased the cRNA concentration up to 3 μg/μl (data not shown). Instead of rendering the chimera NCs non-functional with the pore mutations, we decided to directly co-express the chimeras with WT channels by using the standard cRNA concentration. Therefore, in addition to performing dominant negative assays, we also asked whether chimera NCs could co-assemble with WT channels to generate novel K^+ current phenotypes that cannot be explained by a simple summation of individual current traces. Fig. 11*A* shows that hErg-chimera NC, but not rEag1-chimera NC, exerted a significant current suppression effect on rEag1-WT. In addition, co-expression with hErg-chimera NC resulted in a prominent deceleration of the activation kinetics of rEag1-WT (Fig. 11*A*). By contrast, hErg-chimera NC did not display a notable dominant negative or kinetic effect on hErg-WT (Fig. 11*B*). Most strikingly, co-expression of hErg-WT with rEag1-chimera NC led to a novel K^+ current phenotype that was

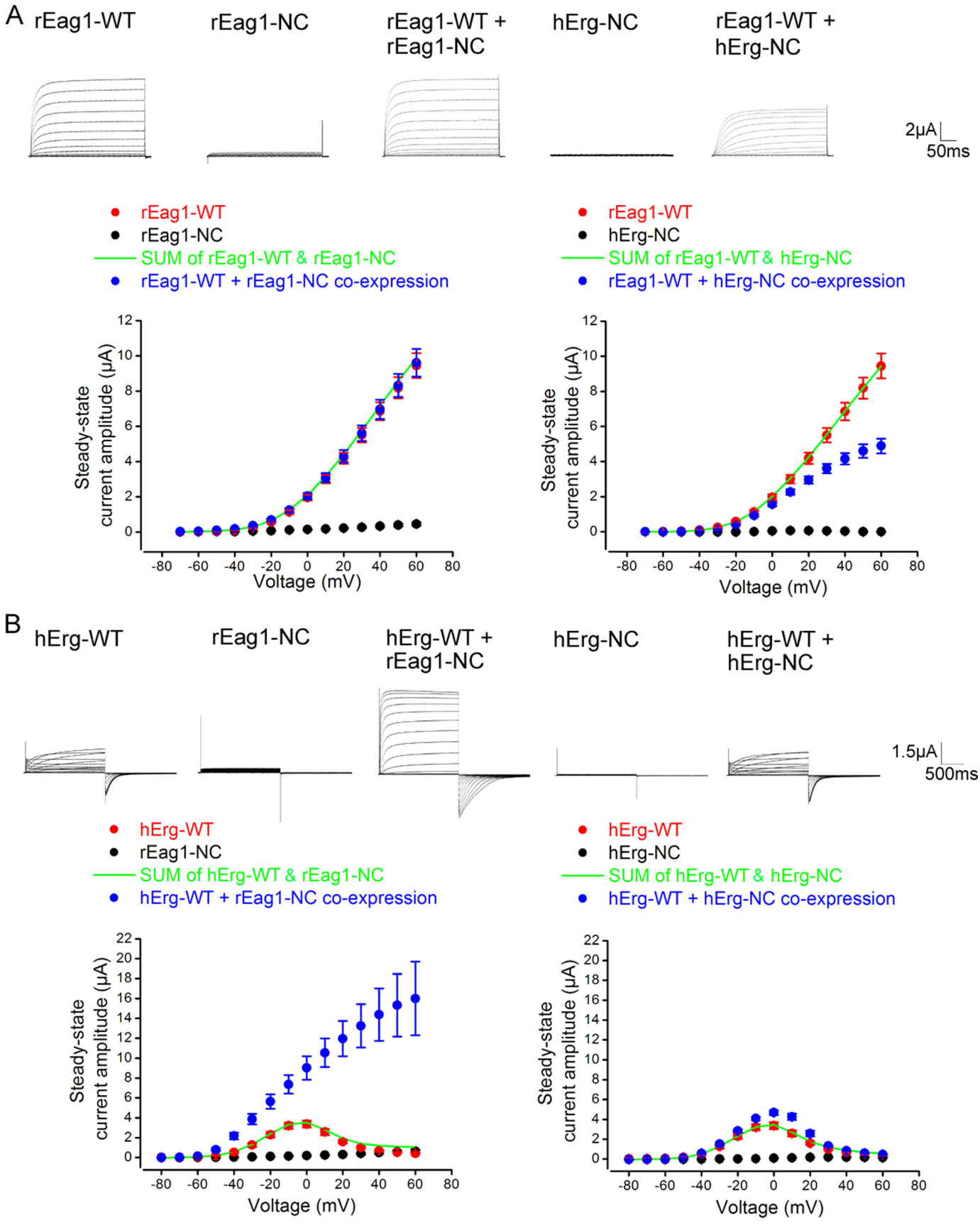
A
rEag1-WT
rEag1-NC
rEag1-WT + rEag1-NC
hErg-NC
rEag1-WT + hErg-NC
2μA
50ms
rEag1-WT
rEag1-NC
SUM of rEag1-WT & rEag1-NC
rEag1-WT + rEag1-NC co-expression
Steady-state current amplitude (μA)
Voltage (mV)
rEag1-WT
hErg-NC
SUM of rEag1-WT & hErg-NC
rEag1-WT + hErg-NC co-expression
Steady-state current amplitude (μA)
Voltage (mV)
B
hErg-WT
rEag1-NC
hErg-WT + rEag1-NC
hErg-NC
hErg-WT + hErg-NC
1.5μA
500ms
hErg-WT
rEag1-NC
SUM of hErg-WT & rEag1-NC
hErg-WT + rEag1-NC co-expression
Steady-state current amplitude (μA)
Voltage (mV)
hErg-WT
hErg-NC
SUM of hErg-WT & hErg-NC
hErg-WT + hErg-NC co-expression
Steady-state current amplitude (μA)
Voltage (mV)

characterized by a dramatic reduction of hErg inactivation and a remarkable deceleration of hErg deactivation (Fig. 11*B*). A similar K^+ current phenotype was also observed when hErg-WT was co-expressed with rEag1-chimera C (Fig. 12*A*), the chimera known to interact with both rEag1 and hErg (see Fig. 4). In comparison, both hErg-chimera B and rEag1-chimera E were unable to cross the boundary of subfamily specificity (see Figs. 4 and 5) and therefore failed to significantly alter the functional expression of rEag1-WT and hErg-WT, respectively (Fig. 12*B*). Taken together, our data are consistent with the idea that both the N-terminal and the C-terminal regions are required to confer the subfamily-specific assembly of rEag1 and hErg subunits.

DISCUSSION

In the current study, we investigated the mechanism underlying the subfamily-specific assembly of rEag1 and hErg K^+ channels. By characterizing the subunit interaction properties of a series of different chimeric and truncation constructs over the C-terminal region, we confirmed the previous report that the CAD/TCC-containing post-CNBHD region may serve as a subfamily recognition domain. On the other hand, we also demonstrated that the C-terminal subfamily recognition domain is actually dispensable for the subunit-specific assembly of rEag1 and hErg. Furthermore, we provided several lines of evidence indicating the presence of a putative N-terminal subfamily recognition domain. Importantly, exchanging either the N-terminal or the C-terminal recognition domain alone did not result in a reversal of subfamily specificity but rather led to a virtual loss of the intersubfamily boundary between rEag1 and hErg. Finally, our biochemical and electrophysiological analyses strongly suggested that both the N-terminal and the C-terminal domains need to be present in order to execute the subunit discrimination task and thereby sustain the subfamily-specific assembly.

To the best of our knowledge, this is the first report showing that the N-terminal region may serve as a subfamily recognition domain for ether-à-go-go K^+ channels. This N-terminal subunit interaction does not seem to be required for the homotetrameric assembly of ether-à-go-go K^+ channel subunits because N-terminal deletions involving the complete eag domain and the majority of the adjacent N-linker region still produced functional K^+ channels for both mouse Eag1 and hErg (31, 35). Likewise, effective subunit interaction within the same subfamily was observed for rEag1 and hErg truncation mutants lacking the CAD and the TCC domain, respectively (16–21), indicating that the putative C-terminal recognition domain is not required for the homotetrameric assembly of ether-à-go-go K^+ channel subunits either. In addition, at least in our heterologous expression system, the molecular control system for subfamily-specific interactions seems to be satisfied with the presence of either one of the two recognition domains, as exemplified by the observation that both the N-terminal and the C-terminal truncation mutants retained their native subfamily specificity.

Overall, we propose that, similar to the formation of heterooligomers by hErg 1a and 1b (34), the subfamily recognition procedure for ether-à-go-go K^+ channels takes place early in the biogenesis process. This subunit recognition task may require concerted interactions of N/C-terminal subfamily-specific sequences, such as the previously identified tetramerizing coiled-coil structure in CAD/TCC (14, 15). We speculate that both the N-terminal and the C-terminal regions serve as equally important subfamily recognition domains that can take over the subfamily discrimination duty in the absence of one or the other. This conjecture may also explain why the chimeras harboring mixed recognition domains from the two subfamilies (*i.e.* chimera Cs, chimera Gs, and chimera Ns) could break the intersubfamily boundary and co-assembled with both rEag1-WT and hErg-WT. For Kv1 channels, intersubunit associations via the T1 domain are considered the initial step of tetramerization during the biogenesis and may not be required for subsequent steps in channel assembly (27, 36). It is therefore likely that once the initial subfamily recognition process is accomplished, the ensuing protein maturation process leading to the tetrameric organization of a functional ether-à-go-go K^+ channel may instead involve subunit assembly via other protein domains, such as the S6-C-linker region (16).

The detailed structural basis underlying the N-terminal recognition domain remains elusive. Based on our finding that the subfamily barrier-breaking phenotypes of chimera Ns could not be properly reproduced when we swapped partial N-terminal sequences only (*i.e.* chimera Ps and chimera Os), we speculate that the N-terminal subfamily recognition domain comprises a subset of protein sequences involving both the distal eag domain and the proximal N-linker region. Alternatively, one may also argue that the N-terminal recognition domain predominantly resides in either the eag domain or the N-linker region only and that the introduction of chimeric sequences in the other part of the N-terminal region may somehow indirectly disrupt the structure of the recognition domain *per se*,

FIGURE 11. **Reversal of subfamily specificity for rEag1- and hErg-chimera NC.** *A*, co-expression of rEag1-WT with rEag1- or hErg-chimera NC in *Xenopus* oocytes. *Top panels*, representative current traces (3 mM external KCl) of various expression conditions. In accord with Fig. 10*A*, both rEag1- and hErg-chimera NC produced negligible K^+ current in 0.1 μg/μl cRNA. In the presence of hErg-chimera NC, the activation kinetics and current amplitude of rEag1-WT were slower and smaller, respectively. *Bottom panels*, steady-state current-voltage relationships of rEag1-WT in the absence (*red circles*) or presence (*blue circles*) of rEag1-chimera NC (*left*) and hErg-chimera NC (*right*). Also shown are the theoretical current-voltage lines derived from a direct sum of corresponding mean current amplitudes of rEag1-WT and chimera NC (*SUM of rEag1-WT & rEag1-NC/hErg-NC*; *green lines*). The current-voltage relationship of rEag1-WT in the presence of rEag1-chimera NC (*rEag1-WT + rEag1-NC co-expression*) was virtually identical to that predicted by the theoretical summation, whereas co-expression with hErg-chimera NC led to a significant reduction of rEag1-WT current amplitudes. *B*, co-expression of hErg-WT with rEag1- or hErg-chimera NC. *Top panels*, representative current traces of various expression conditions. Upon co-expression with rEag1-chimera NC, hErg-WT manifested non-inactivating outward K^+ currents, followed by notably slower tail current kinetics. *Bottom panels*, current-voltage relationships of hErg-WT in the absence (*red circles*) or presence (*blue circles*) of rEag1-chimera NC (*left*) and hErg-chimera NC (*right*) as well as the theoretical summation line (*SUM of hErg-WT & rEag1-NC/hErg-NC*; *green lines*). The current-voltage relationship of hErg-WT in the presence of hErg-chimera NC (*hErg-WT + hErg-NC co-expression*) agreed with that predicted by the theoretical summation, whereas co-expression with rEag1-chimera NC resulted in a significant augmentation of hErg-WT current amplitudes. For both chimera NCs (*black circles*), the values of S.E. were smaller than those of mean. Data were averaged from 6–14 oocytes. *Error bars*, S.E.

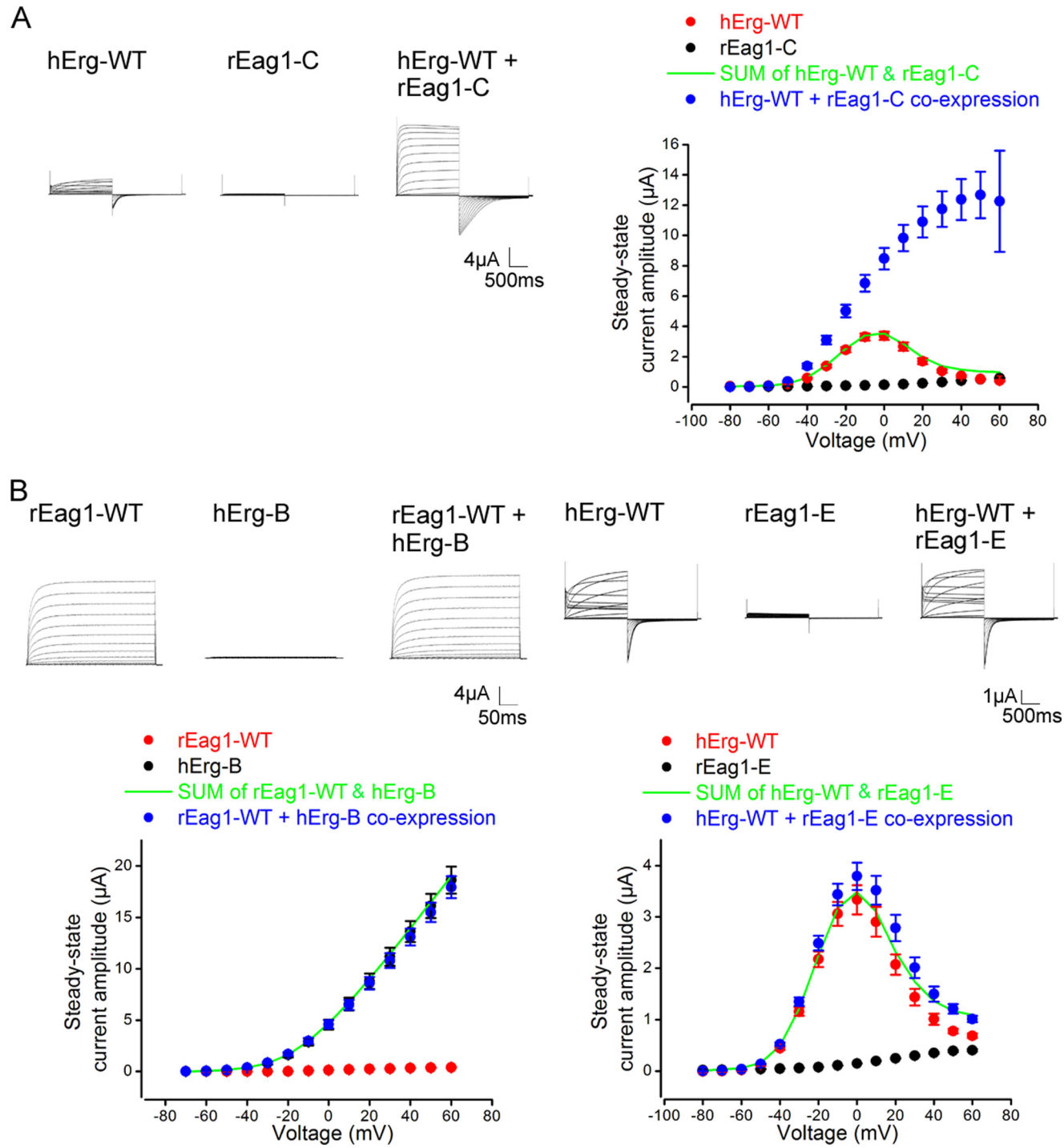

FIGURE 12. **Alteration of hErg-WT functional phenotype by rEag1-chimera C.** *A*, co-expression of hErg-WT with rEag1-chimera C in *Xenopus* oocytes; representative current traces (*left*) and current-voltage relationships (*right*). Co-expression of hErg-WT and rEag1-chimera C manifested non-inactivating outward currents and remarkably slower tail kinetics. *B*, co-expression of rEag1-WT and hErg-chimera B (*left panels*) and of hErg-WT and rEag1-chimera E (*right panels*). In either case, co-expression with the chimera failed to noticeably affect the current amplitude and kinetics of the corresponding WT channel. Data were collected from 5–12 oocytes. *Error bars*, S.E.

thereby abolishing or reducing its subfamily differentiation efficacy. Regardless of its physical nature, the N-terminal recognition domain as well as the C-terminal counterpart should be able to effectively promote or stabilize the initial assembly of structurally compatible ether-à-go-go K^+ channel subunits in a manner similar to what has previously been proposed for the T1 domain in Kv1 channels (27). It remains to be determined, however, how the N-terminal and the C-terminal domains coordinate with each other during the subunit recognition process in the endoplasmic reticulum. One possibility is that they accomplish this task in a sequential and perhaps independent manner, with the N-terminal domain initiating a co-translational association procedure. Alternatively, given that in mature tetrameric Eag1 and hErg proteins, the N-terminal eag domain

seems to be able to physically interact with the C-terminal CNBHD (26, 30, 37, 38), the initial subunit recognition process mediated by the N-terminal domain may be subject to further modification dictated by the C-terminal domain.

In KCNQ (Kv7) channels, subunit interaction and subtype-specific assembly have been shown to be determined by two coiled-coil domains in the distal C-terminal region (39). Moreover, other members of the CNBHD-containing channel family such as cyclic nucleotide-gated cation channels and plant inward rectifying AKT1/KAT1 K^+ channels (40–42). As in the case for ether-à-go-go K^+ channels, their N-terminal regions have long been postulated not to contribute to intersubunit assembly, although little experimental evidence was provided to support this assumption. The findings from our study would thus open up interesting perspectives for future investigations into the possibility that the subfamily-specific assembly of these channels may also employ both N-terminal and C-terminal recognition domains.

In summary, the current study provides compelling evidence showing that both the N-terminal and the C-terminal regions are required to confer the subfamily-specific assembly of rEag1 and hErg subunits. This requirement for compatible subfamily-specific interactions in both the N-terminal and the C-terminal recognition domains may ensure a better control against erroneous intersubfamily assembly. The physiological significance of our findings is highlighted by the fact that virtually all members of the ether-à-go-go K^+ channel family display an abundant expression in the mammalian brain, in which a wide variety of different voltage-gated K^+ channels contribute to diverse brain functions based on distinct subunit-specific subcellular targeting to precise sites and compartments in the neuronal membrane (43). The presence of a stringent molecular control system against intersubfamily heterotetramer formation is therefore crucial for the differential subcellular localization of discrete ether-à-go-go subunits in neurons.

Acknowledgment—We thank Dr. Chih-Yung Tang for technical guidance and for critically reading the manuscript.

REFERENCES

1. Hille, B. (2001) *Ion Channels of Excitable Membranes*, 2nd Ed., pp. 131–167, Sinauer, Sunderland, MA
2. Johnston, J., Forsythe, I. D., and Kopp-Scheinpflug, C. (2010) Going native: voltage-gated potassium channels controlling neuronal excitability. *J. Physiol.* **588,** 3187–3200
3. MacKinnon, R. (1991) Determination of the subunit stoichiometry of a voltage-activated potassium channel. *Nature* **350,** 232–235
4. Liman, E. R., Tytgat, J., and Hess, P. (1992) Subunit stoichiometry of a mammalian K^+ channel determined by construction of multimeric cDNAs. *Neuron* **9,** 861–871
5. Gutman, G. A., Chandy, K. G., Grissmer, S., Lazdunski, M., McKinnon, D., Pardo, L. A., Robertson, G. A., Rudy, B., Sanguinetti, M. C., Stühmer, W., and Wang, X. (2005) International Union of Pharmacology. LIII. Nomenclature and molecular relationships of voltage-gated potassium channels. *Pharmacol. Rev.* **57,** 473–508
6. Covarrubias, M., Wei, A. A., and Salkoff, L. (1991) Shaker, Shal, Shab, and Shaw express independent K^+ current systems. *Neuron* **7,** 763–773
7. Isacoff, E. Y., Jan, Y. N., and Jan, L. Y. (1990) Evidence for the formation of heteromultimeric potassium channels in *Xenopus* oocytes. *Nature* **345,** 530–534
8. Li, M., Jan, Y. N., and Jan, L. Y. (1992) Specification of subunit assembly by the hydrophilic amino-terminal domain of the Shaker potassium channel. *Science* **257,** 1225–1230
9. Deal, K. K., Lovinger, D. M., and Tamkun, M. M. (1994) The brain Kv1.1 potassium channel: *in vitro* and *in vivo* studies on subunit assembly and posttranslational processing. *J. Neurosci.* **14,** 1666–1676
10. Shen, N. V., and Pfaffinger, P. J. (1995) Molecular recognition and assembly sequences involved in the subfamily-specific assembly of voltage-gated K^+ channel subunit proteins. *Neuron* **14,** 625–633
11. Shen, N. V., Chen, X., Boyer, M. M., and Pfaffinger, P. J. (1993) Deletion analysis of K^+ channel assembly. *Neuron* **11,** 67–76
12. Warmke, J. W., and Ganetzky, B. (1994) A family of potassium channel genes related to eag in *Drosophila* and mammals. *Proc. Natl. Acad. Sci. U.S.A.* **91,** 3438–3442
13. Wimmers, S., Wulfsen, I., Bauer, C. K., and Schwarz, J. R. (2001) Erg1, erg2 and erg3 K channel subunits are able to form heteromultimers. *Pflugers Arch.* **441,** 450–455
14. Ludwig, J., Owen, D., and Pongs, O. (1997) Carboxy-terminal domain mediates assembly of the voltage-gated rat ether-a-go-go potassium channel. *EMBO J.* **16,** 6337–6345
15. Jenke, M., Sánchez, A., Monje, F., Stühmer, W., Weseloh, R. M., and Pardo, L. A. (2003) C-terminal domains implicated in the functional surface expression of potassium channels. *EMBO J.* **22,** 395–403
16. Chen, I. H., Hu, J. H., Jow, G. M., Chuang, C. C., Lee, T. T., Liu, D. C., and Jeng, C. J. (2011) Distal end of carboxyl terminus is not essential for the assembly of rat Eag1 potassium channels. *J. Biol. Chem.* **286,** 27183–27196
17. Akhavan, A., Atanasiu, R., and Shrier, A. (2003) Identification of a COOH-terminal segment involved in maturation and stability of human ether-a-go-go-related gene potassium channels. *J. Biol. Chem.* **278,** 40105–40112
18. Aydar, E., and Palmer, C. (2001) Functional characterization of the C-terminus of the human ether-a-go-go-related gene K^+ channel (HERG). *J. Physiol.* **534,** 1–14
19. Li, X., Xu, J., and Li, M. (1997) The human Δ1261 mutation of the HERG potassium channel results in a truncated protein that contains a subunit interaction domain and decreases the channel expression. *J. Biol. Chem.* **272,** 705–708
20. Gong, Q., Keeney, D. R., Robinson, J. C., and Zhou, Z. (2004) Defective assembly and trafficking of mutant HERG channels with C-terminal truncations in long QT syndrome. *J. Mol. Cell Cardiol.* **37,** 1225–1233
21. Choe, C. U., Schulze-Bahr, E., Neu, A., Xu, J., Zhu, Z. I., Sauter, K., Bähring, R., Priori, S., Guicheney, P., Mönnig, G., Neapolitano, C., Heidemann, J., Clancy, C. E., Pongs, O., and Isbrandt, D. (2006) C-terminal HERG (LQT2) mutations disrupt IKr channel regulation through 14–3-3ε. *Hum. Mol. Genet.* **15,** 2888–2902
22. Chuang, C. C., Jow, G. M., Lin, H. M., Weng, Y. H., Hu, J. H., Peng, Y. J., Chiu, Y. C., Chiu, M. M., and Jeng, C. J. (2014) The punctate localization of rat Eag1 K^+ channels is conferred by the proximal post-CNBHD region. *BMC Neurosci.* **15,** 23
23. Curran, M. E., Splawski, I., Timothy, K. W., Vincent, G. M., Green, E. D., and Keating, M. T. (1995) A molecular basis for cardiac arrhythmia: HERG mutations cause long QT syndrome. *Cell* **80,** 795–803
24. Schönherr, R., Gessner, G., Löber, K., and Heinemann, S. H. (2002) Functional distinction of human EAG1 and EAG2 potassium channels. *FEBS Lett.* **514,** 204–208
25. Brelidze, T. I., Carlson, A. E., Sankaran, B., and Zagotta, W. N. (2012) Structure of the carboxy-terminal region of a KCNH channel. *Nature* **481,** 530–533
26. Gustina, A. S., and Trudeau, M. C. (2011) hERG potassium channel gating is mediated by N- and C-terminal region interactions. *J. Gen. Physiol.* **137,** 315–325
27. Zerangue, N., Jan, Y. N., and Jan, L. Y. (2000) An artificial tetramerization domain restores efficient assembly of functional Shaker channels lacking T1. *Proc. Natl. Acad. Sci. U.S.A.* **97,** 3591–3595
28. Morais Cabral, J. H., Lee, A., Cohen, S. L., Chait, B. T., Li, M., and Mackinnon, R. (1998) Crystal structure and functional analysis of the HERG potassium channel N terminus: a eukaryotic PAS domain. *Cell* **95,** 649–655
29. Sahoo, N., Tröger, J., Heinemann, S. H., and Schönherr, R. (2010) Current

inhibition of human EAG1 potassium channels by the Ca^{2+} binding protein S100B. *FEBS Lett.* **584,** 3896–3900
30. Haitin, Y., Carlson, A. E., and Zagotta, W. N. (2013) The structural mechanism of KCNH-channel regulation by the eag domain. *Nature* **501,** 444–448
31. Viloria, C. G., Barros, F., Giráldez, T., Gómez-Varela, D., and de la Peña, P. (2000) Differential effects of amino-terminal distal and proximal domains in the regulation of human erg K^+ channel gating. *Biophys. J.* **79,** 231–246
32. Lees-Miller, J. P., Kondo, C., Wang, L., and Duff, H. J. (1997) Electrophysiological characterization of an alternatively processed ERG K^+ channel in mouse and human hearts. *Circ. Res.* **81,** 719–726
33. London, B., Trudeau, M. C., Newton, K. P., Beyer, A. K., Copeland, N. G., Gilbert, D. J., Jenkins, N. A., Satler, C. A., and Robertson, G. A. (1997) Two isoforms of the mouse ether-a-go-go-related gene coassemble to form channels with properties similar to the rapidly activating component of the cardiac delayed rectifier K^+ current. *Circ. Res.* **81,** 870–878
34. Phartiyal, P., Jones, E. M., and Robertson, G. A. (2007) Heteromeric assembly of human ether-a-go-go-related gene (hERG) 1a/1b channels occurs cotranslationally via N-terminal interactions. *J. Biol. Chem.* **282,** 9874–9882
35. Carlson, A. E., Brelidze, T. I., and Zagotta, W. N. (2013) Flavonoid regulation of EAG1 channels. *J. Gen. Physiol.* **141,** 347–358
36. Lu, J., Robinson, J. M., Edwards, D., and Deutsch, C. (2001) T1-T1 interactions occur in ER membranes while nascent Kv peptides are still attached to ribosomes. *Biochemistry* **40,** 10934–10946
37. Stevens, L., Ju, M., and Wray, D. (2009) Roles of surface residues of intracellular domains of heag potassium channels. *Eur. Biophys. J.* **38,** 523–532
38. Muskett, F. W., Thouta, S., Thomson, S. J., Bowen, A., Stansfeld, P. J., and Mitcheson, J. S. (2011) Mechanistic insight into human ether-a-go-go-related gene (hERG) K^+ channel deactivation gating from the solution structure of the EAG domain. *J. Biol. Chem.* **286,** 6184–6191
39. Haitin, Y., and Attali, B. (2008) The C-terminus of Kv7 channels: a multifunctional module. *J. Physiol.* **586,** 1803–1810
40. Daram, P., Urbach, S., Gaymard, F., Sentenac, H., and Cherel, I. (1997) Tetramerization of the AKT1 plant potassium channel involves its C-terminal cytoplasmic domain. *EMBO J.* **16,** 3455–3463
41. Dreyer, I., Poree, F., Schneider, A., Mittelstädt, J., Bertl, A., Sentenac, H., Thibaud, J. B., and Mueller-Roeber, B. (2004) Assembly of plant Shaker-like K(out) channels requires two distinct sites of the channel α-subunit. *Biophys. J.* **87,** 858–872
42. Zhong, H., Molday, L. L., Molday, R. S., and Yau, K. W. (2002) The heteromeric cyclic nucleotide-gated channel adopts a 3A:1B stoichiometry. *Nature* **420,** 193–198
43. Vacher, H., Mohapatra, D. P., and Trimmer, J. S. (2008) Localization and targeting of voltage-dependent ion channels in mammalian central neurons. *Physiol. Rev.* **88,** 1407–1447